JIMMA UNIVERSITY

SCHOOL OF GRADUATE STUDIES

DEPARTMENT OF CHEMISTRY

SYNTHESIS OF ZINC OXIDE NANOPARTICLES AND COBALT DOPED ZINC OXIDE NANOCOMPOSITES USING *Allium cepa L. AQEOUS* PEEL EXTRACT AND EVALUATION OF ITS ANTIMICROBIAL AND PHOTOCATALYTIC ACTIVITIES

BY: MISGANA AGASA

ADVISOR: GUTA GONFA (Ph.D)

CO-ADVISOR: KIRUBEL TESHOME (Ph.D Candidate)

MAY, 2023

JIMMA, ETHIOPIA

SYNTHESIS OF ZINC OXIDE NANOPARTICLES AND COBALT DOPED ZINC OXIDE NANOCOMPOSITES USING *Allium cepa L*. AQEOUS PEEL EXTRACT AND EVALUATION OF ITS ANTIMICROBIAL AND PHOTOCATALYTIC ACTIVITIES

A THESIS SUBMITTED TO THE SCHOOL OF GRADUATE STUDIES OF JIMMA UNIVERSITY IN PARTIAL FULFILMENT OF THE REQUIREMENTS FOR THE DEGREE OF MASTERS OF SCIENCE IN CHEMISTRY

BY:

MISGANA AGASA

ADVISOR

GUTA GONFA (Ph.D)

CO-ADVISOR

KIRUBEL TESHOME (Ph.D Candidate)

MAY, 2023

JIMMA, ETHIOPIA

JIMMA UNIVERSITY

COLLEGE OF NATURAL SCIENCES

MSc THESIS APPROVAL SHEET

We, the undersigned, member of the Board of Examiners of the final open defense by **Misgana Agasa** have read and evaluated his/her thesis entitled "**Synthesis of Zinc Oxide Nanoparticles and Cobalt doped Zinc Oxide Nanocomposites using *Allium cepa* l. Aqueous peel extract and evaluation of its Antimicrobial and Photocatalytic Activities**" and examined the candidate. This is therefore to certify that the thesis has been accepted in partial fulfillment of the requirements for the degree Master of Science in **Chemistry**

Gebru G /Tsadik (MSc)	_____	_____
Name of the Chairperson	Signature	Date
Gutta Gonfa Ph.D.)	_____	_____
Name of Major Advisor	Signature	Date
Tsegaye Girma (Ph.D.)	_____	_____
Name of the Internal Examiner	Signature	Date
Raji Feyisa (Ph.D.)	_____	_____
Name of the External Examiner	Signature	Date
_____	_____	_____
Department Head	Signature	Date

Declaration

I declare that the work described in this thesis is my original work under the supervision of my advisors, Dr. Guta Gonfa (Ph.D) and Kirubel Teshome (Ph.D candidate) at the Department of Chemistry, Jimma University for the degree of M.Sc. in Chemistry.

I also declare that the substance of this thesis has neither been submitted elsewhere nor is being currently submitted for any other degree.

I further declare that the thesis embodies the results of my research or advanced studies and that it has been composed by me. Where appropriate I had acknowledged the work of others.

Name: MISGANA AGASA Signature: _____ Date_____

Graduate Thesis Ownership Agreement

This thesis is a property of Jimma University, an institution that awarded **MSc** Degree to the graduate student and funded its research cost fully or partly. The research work was accomplished under the close support and supervision of the assigned University's academic staff. It is therefore strictly forbidden to publish, modify, or communicate to or put at the disposal of third party the entire document or any part thereof without the common consent of the research supervisor(s) and the graduate student. Disregarding this agreement would lead to accountability according to the Jimma University's Research and Publication Misconduct Policy **Article 1.7** of the University's Document for "Guidelines and Procedures for Research, March
2012".

Name of the Graduate Student Signature Date

_____ _____ _____

Name (s) of the Research Supervisor (s) Signature Date

_____ _____ _____

_____ _____ _____ _____

Title of the Thesis:

_____

_____

Degree Awarded: Msc.

College of Natural Sciences, Jimma University

ACKNOWLEDGMENT

First and foremost, I offer my thanks to Almighty God, who has helped me throughout my life. Secondly, I wish to express my deepest gratitude and sincere thanks to my honorable advisor, Dr. Guta Gonfa, Department of Chemistry, Jimma University College of Natural Science, for providing me with the opportunity to work under his guidance. His kind attention, patience, care, motivating discussions, sustained interest, and continuous encouragement have been a source of inspiration for me throughout this research. I appreciate his contributions of time and productive criticism to complete the task. Next, I would like to thank my co -nks to Almighty God, who has helped me throughout my life. Second, a special thanks to my mother for her continuous support and understanding throughout this journey. Frankly, this work would not have been completed without her motivation and encouragement, even in very knotty situations from beginning to end, and so I have heartfelt thanks for her. I wish to express my deepest gratitude and sincere thanks to my honorable advisor, Dr. Guta Gonfa, Department of Chemistry, Jimma University College of Natural Science, for providing me with the opportunity to work under his guidance. His kind attention, patience, care, motivating discussions, sustained interest, and continuous encouragement has been a source of inspiration for me throughout this research. I appreciate his contributions of time and productive criticism to complete the task. Next, I would like to thank my co-advisor, Kirubel Tashome (Ph.D candidate), for his scientific guidance, support, and motivation during the work of this thesis, especially at the beginning. A special thanks to my mother for her continuous support and understanding throughout this journey. Frankly, this work would not have been completed without her motivation and encouragement, even in very knotty situations from beginning to end, and so I have heartfelt thanks to her. Entirely, their support, care, and training made me capable of tackling various situations. I will always remember their personal cooperation, encouragement, and polite manner with me in every situation during my research. Finally, I am extremely grateful to my other respected bodies as well as Jimma University for providing different facilities for their intellectual help and continuous inspiration throughout my research work.

ABSTRACT

Since dye effluents discharged from different industries lead to environmental contamination, their treatment and environmental remediation are highly desired. Due to the limitations of physical treatment methods like adsorption, photocatalytic degradation was used because of its capability to complete the degradation of dyes. On the other hand, most microbial species have shown resistance to antibiotic drugs. Concerning this, nanomaterials have been found to be a promising candidate to overcome such a problem. Metal oxide-based nanostructures are widely used in photochemical processes and antimicrobial agents due to their unique properties. But single-nanostructure metal oxide materials might suffer from low efficiency under visible light. This fact makes it important to have efficient and reliable nanocomposites for the photochemical processes. The combination of different nanomaterials to form a composite configuration can produce a material with new properties. The new properties, which are due to the synergetic effect, are a combination of the properties of all the counterparts of the nanocomposites. The main objective of this research was to synthesize ZnO NPs and Co/ZnO NCs by precipitation using red onion peel plant aqueous extract for photocatalytic and antimicrobial applications. Co/ZnO NCs were prepared from red onion peel plant aqueous extract , $Zn(NO_3)_2$.$6H_2O$) and $Co(NO_3)_2.6H_2O$ solution at 65 ^{0}C for 2 h and ZnO NPs were prepared in the same way, but without the addition of $Co(NO_3)_2.6H_2O$ solution. The synthesized ZnO NPs and Co/ZnO NCs were characterized by UV-Vis, XRD, FT-IR, and SEM techniques. From the UV-Vis absorption spectrum, the peaks of ZnO NPs and Co/ZnO NCs were detected at 369 and 375 nm, respectively. The XRD data showed the crystalline nature of the NPs and NCs, and the average crystallite size of ZnO NPs and Co-ZnO NCs is 27.47 and 33.97, respectively. The FT-IR result revealed the presence of important functional groups like tannins and phenolics, which were also observed in the phytochemical screening test experiment. The SEM result showed hexagonal wurtzite and spherical-like morphologies for ZnO Nps and Co/ZnO NCs, respectively. The in vitro antimicrobial test of NMs showed good antimicrobial activity, especially at high concentrations. The result indicates that Co/ZnO NCs showed enhanced antimicrobial activity compared to ZnO NPs. The photocatalytic performance of Co/ZnO NCs was further assessed by the degradation of MB dye as a model pollutant under irradiation of natural sunlight and compared with that of bare ZnO NPs. The effect of some parameters like pH, catalyst dosage, irradiation time, and initial dye concentration of MB dye on the activity of Co/ZnO NCs was also

investigated. 98.5% and 89.3% of MB dye were degraded by Co/ZnO NCs and ZnO NPs at 60 min, which is a promising future application of solar light driven photocatalytic degradation of organic pollutants.

Keywords*: Allium cepa L*, antimicrobial, photocatalytic, zinc oxide nanoparticles, cobalt-doped zinc oxide nanocomposites

LIST OF ABBREVIATIONS AND ACRONYMS

CB	Conduction Band
eV	Electron volt
FT-IR	Fourier transform infrared
MB	Methylene blue
NCs	Nanocomposites
NPs	Nanoparticles
ppm	Parts per million
ppb	Parts per billion
PE	Plant Extract
RNS	Reactive Nitrogen Species
ROP	Red Onion Peel
ROS	Reactive Oxygen Species
SEM	Scanning Electron Microscopy
VB	Valance Band
XRD	X-Ray Diffraction

Table of Contents

List of tables

List of figures

1. INTRODUCTION

1. 1. Background of the study

Microorganisms are important for a wide range of life-sustaining functions. On the other hand, some are pathogenic, meaning they can cause illness and even death. The super bacteria and fungi are types of microbial strains that show resistance against all the antibiotics, which have been developed recently because of the abuse of antibiotics [1]. Currently, both gram-positive and gram-negative bacterial strains are considered the primary cause of major public health problems all over the world, which requires a significant solution [2]. *Escherichia coli* (*E*. coli), a natural inhabitant of the intestine and part of the intestinal fora, has a distinctive position in the microbiological world due to its potential virulent properties and challenge for food safety and security [3]. *Bacillus* species that produce subtilin and subtilosin will cause two types of illness, like diarrhea and vomiting. *Staphylococcus aureus* (*S. aureus*) is a common pathogenic bacterium responsible for up to 40% of mastitis cases in dairy animals [4, 5]. On top of that, currently, fungal infections afflict more than a billion individuals globally. *Candida albicans* is the most prevalent fungal pathogen and is responsible for a significant proportion of oral candidiasis cases. The pharmaceutical and medical industries have prepared various types of antibiotics to control these diseases; however, these antibiotics, sometimes lead to antagonistic/allergic side effects and infections [6, 7].

With the emergence of microorganisms resistant to multiple antimicrobial agents, there is a growing interest in developing new bactericides and fungicides using nanotechnology based on nanomaterials [8]. Nanoparticles (NPs) are progressively utilized to target bacteria and fungi as contrasting options to antibiotics [9].

On the other hand, nowadays, the effluent of dyes from different industries in their production processes poses a challenge for environmental safety. Dyes usually have a synthetic origin and complex aromatic molecular structures, which make them more stable and more difficult to biodegrade [10]. Several conventional methods, including flocculation, precipitation, adsorption, and so forth, have been used for the treatment of wastewater; however, these methods cannot completely degrade the organic pollutants because of the

high stability of the dyes towards the oxidizing agents, which results in inadequate removal of toxic compounds. Therefore, advanced methods, mainly using harmless semiconductors (especially those of transition metal oxides) of inorganic nanomaterials such as nanoparticles and their composites possessing strong chemo-reactive potential, are used for the photocatalytic degradation of synthetic organic dyes [11, 12].

Among the various transition metal oxide semiconductor nanostructures, ZnO nanostructures have attracted considerable interest because of their amazing advantages, such as bio-safety, lower cost, and high chemical and physical stability [9–12]. These characteristics make ZnO a promising material for a number of applications, such as gas sensors, antibacterial coatings, photocatalytic degradation of organic pollutants, electrical devices, optical coatings, and solar cells, which are extensively used in the fields of biomedical research, optics, and electronics. Besides the good properties of ZnO NPs, intrinsic ZnO cannot be directly utilized as an effective photocatalytic and antimicrobial material, which is due to the countable ZnO drawbacks such as lack of visible light absorption, agglomeration, and poor optical properties [13, 14].

Among the different techniques reported to overcome this constraint, doping is the most important and simple method. Doping is related to the intentional introduction of impurities into a pure material for the purpose of modulating its new properties. Cobalt is a vital element that is present in small quantities in the body of a mammal and is usually provided in a diet of green vegetables and grains. Key among its biological activities is its role in vitamin B_{12}, cobalamin, as well as in a small amount of other cobalt-containing enzymes identified to date. Due to the importance of cobalt in the human metabolic process, various materials based on cobalt suitable for biomedical purposes are becoming more common [35]. Co^{2+} is chosen as an impurity element (dopant) because it is the most common transition metal element expected to modify the photocatalytic effect and antimicrobial activity of ZnO nanoparticles, due to the fact that Shannon's effective ionic radii for tetrahedrally coordinated Zn^{2+} and Co^{2+} are similar to each other, 0.74 and 0.72 Å, respectively [15–17].

Plant phytochemicals, through the green method, have been extensively used to synthesize metal oxide NPs. This is because of their abundance, safe nature, as well as the greater stabilization and reduction of metal ions to zerovalent metal atoms. This method has been

considered an alternative to complex and costly physicochemical processes because of the following properties: viability, eco-friendliness, reliability, no waste generation, simplicity [18, 19], biocompatibility, low energy requirement, rapid synthesis, ease of processing, easy scale-up, and sustainable stability of synthesized nanoparticles. Onion processing waste mainly includes skin (peel), and various onions (white, yellow, and red) contain large amounts of bioactive compounds such as phenolics, favonoids, and anthocyanins. However, the amount of these compounds in red onions is higher than that in other onions, and the amounts in the skin of red onions are higher than those in their edible parts [22, 23]. Valorization is widely applied to managing agro-industrial by-products, in which by-products are considered valuable secondary raw materials with potential functional constituents for developing value-added products [24]. fig .1

Fig 1. A, plant peel, and B, plant peel powder of *Allium cepa* L.

Many researchers have reported the green synthesis of ZnO NPs and transition metal-doped ZnO NCs using different plant extracts such as lemongrass, Madhuca longifolia, Aspergillus fumigates, Nerium oleander, Bifurcaria bifurcate, Euphorbia esula, Albizia lebbeck, and Lantana camara [24, 25]. There were only a few research studies reported on red onion peel extract-mediated transition metal-doped ZnO nanomaterials used for photocatalytic degradation of industrial and recalcitrant dyes such as 4-nitrophenol other than MB and antibacterial activities [2]. However, to the best of our knowledge, red onion skin aqueous extract supported (or mediated) green synthesis of cobalt-doped ZnO nanocomposite used for antimicrobial activity and photocatalytic effect for degradation of MB dye as a major pollutant has never been reported yet. Therefore, in this work, we initiated the synthesis of

ZnO NPs and cobalt doped zinc oxide nanocomposite using red onion peel aqoues extract through the green route and evaluated its photocatalytic effect for decolorizations of MB dye and antimicrobial activity against four selected strains of pathogens: two gram positive bacteria (*S. aureus and B. cereus*), one gram negative bacteria *(E. coli),* and one fungus (*C. albican*) for the first time. The various factors that affect the photodegradation of MB dye, such as pH, temperature, catalyst dose, and irradiation time, have been investigated.

1.2. Statement of the problems

The release of synthetic organic dyes such as MB into the environment has been of great concern due to the properties and effects of dye-contaminated water on the environment since most of these dyes are not biodegradable and persistent, harming aquatic as well as non-aquatic life. On top of this, nowadays, multidrug-resistant microorganisms are bringing very great challenges all over the world, particularly in developing countries, due to the development of different mechanisms of drug resistance by these microorganisms, such as bacteria and fungi, and hence adaptations to the drug, such as antibiotics. And so to solve such obstacles, using inorganic nanomaterials is advisable to a great extent because of the astonishing advantages of these materials, such as heat resistance. Additionally, utilizations of wastes such as red onion skin in solving environmental and health problems are still not explored to their full extent, so exploring their use is important as well. Onion waste remains underutilized even though it is a rich source of bioactive compounds such as phenols, flavonoids, and alkaloids. Thus, the valorization of onion waste and its extracts in the biomedicine and pharmaceutical fields can be an apt solution to reduce environmental damage and provide an economical, low-cost substitute for the generation of therapeutic supplements or herbal-based medicines [28].

The bioactivities of these plants can be enhanced more when they are supported with metal/metal oxide NPs. The surface reaction phenomenon of these biosynthesized particles (moiety on the surface) and the high surface area to volume ratio of particles generate a tendency to interact with pathogens. On the other hand, metal/metal oxide nanoparticles play a great role in the removal of toxic pollutants to remediate a safe environment; however, the physical and chemical methods of synthesis of metal oxide NPs are expensive and not eco-friendly. Therefore, bio-synthesized metal oxide NPs and their composites based on green

chemistry perspectives impose limited hazards to the environment and are relatively biocompatible methods for the production of NMs in an eco-friendly manner. The synthesized nanoparticles and composites are expected to have the efficiency to remove toxic dyes and kill the specified microbial species to save the environment and prevent health problems. With the above pieces of evidence, the present research was intended to explore the photocatalytic effect of the plant peel extract supported by Co/ZnO NCs and evaluate their antimicrobial activities.

Based on this, in this study, the following questions have been answered:

1. Do phtochemicals present in the extract are effective for the synthesis of the specified NPs and NCs?
2. Do the synthesized Co/ZnO NCs show potential photocatalytic degradation of dyes and antimicrobial capacity?
3. Is metal doping of metal oxide NPs enhancing the dye degradation activity of the composites?

1.3. Objectives of the study

1.3.1. General Objective

The main objective of this study was to synthesize ZnO NPs and Co/ZnO NCs using *Allium cepa* peel aqueous extract and evaluate their antimicrobial and photocatalytic activities.

1.3.2. Specific objectives

- To prepare the *Allium cepa L.* aqueous peel extract
- To screen the phytochemicals present in the extract
- To synthesize ZnO NPs and Co/ZnO NCs using the *Allium cepa* aqueous peel
- To characterize the synthesized samples using XRD, UV-Vis, FT-IR, and SEM.
- To evaluate the photocatalytic effect and antimicrobial activity of the synthesized Co/ZnO NCs and compare them with undoped ZnO NPs.

1.4. The significance of the study

Green synthesis of nanoparticles was proven to be a better method of synthesis due to slower kinetics, better manipulation, and their stabilization. Synthesizing nanoparticles with the desired size and composition is of great interest as it provide solutions to various health and environmental challenges [29]. Therefore, the synthesized ZnO NPs and Co/NCs using *Allium cepa L* plant peel aqueous extracts may provide the following significance:

1. Enhance knowledge about ZnO NPs and Co/ZnO NCs.
2. The newly synthesized samples may help reduce environmental pollution and health related problems.
3. The newly synthesized samples may help to explore the reuse of *Allium cepa peel* is used as a medicinal substitute and as a source of economy for the society when necessary.

2. REVIEW OF RELATED LITERATURE

2. 1. Nanoscience and Nanotechnology

Nanoscience is a scientific effort towards achieving complete control over the surface of atoms and molecules. Nanotechnology is one of the fields of applied science and technology that is highly concerned with the understanding and control of matter at any of its dimensions, approximately 1 to 100 nanometers (nms) [30].

Exploiting the knowledge of nanotechnology at molecular and atomic levels serves as a basis for applying an integrative approach to develop novel compounds with unique features for use in broad-spectrum applications [19]. Thus, nanotechnology has emerged as a new research field regarding the preparation of nanomaterials such as nanoparticles (NPs) and nanocomposites (NCs) because of their multifunctional properties and efficiency [31].

Nanoscience and nanotechnology are supposed to encompass all fields of science and technology because any material particle is made up of atoms and molecules. The main focus of nanoscience and nanotechnology is synthesis of new nanoparticles with various sizes and morphologies for various applications. Thus, nanoscience and nanotechnology have opened new venues in science and technology [28].

2. 2. Nanoparticles and nanocomposites

Nanoparticles are one class of nanomaterials and are defined as certain complexes of solid units that possess sizes between 1 and 100 nm. The most unusual aspect of nanoparticles is that they retain a large surface area to volume ratio due to the minute size of the particles when compared to their bulk counterparts [32, 33].

Nanocomposites are a type of hybrid material that includes nanoscale reinforcements and a matrix and are multiple phase solid materials having at least one dimension less than 100 nm [28, 34]. A composite material is made by combining two or more materials, which work together to give unique properties. However, each of the materials alone does not have the desired characteristics [25]. Due to nanocomposites' special properties, such as high strength, high rigidity, high durability, low density, high corrosion resistance, gas barrier, and heat resistance, they provide many advantages over other materials [35]. Their distinct functional qualities make them a viable candidate for a variety of applications for

photocatalysis, catalysis, sensor technology, magnetic property, DNA binding, food, engineering, medical, disease diagnosis and treatment, anti-carcinogenic, antioxidant, anti-tubercular, and antimicrobial [36]. Nanoparticles and nanocomposites are a promising platform for alternative strategies to manage bacterial ailments, as they provide long-term antimicrobial activity with minimal toxicity, as opposed to tiny-molecule antimicrobial drugs like antibiotics, which have short-term activity and are hazardous to the environment [37].

When the size of a crystal is decreased to the nanometer range, the electronic structure changes from continuous bands to discrete or quantized electronic levels. Consequently, the continuous optical transitions in the molecule become quantized, and therefore their properties become size-controlled [3]. This in turn leads to changes in chemical features such as electronic, structural, spectroscopic, magnetic, and thermodynamic [4].

The nano-sized particles have a high surface area to volume ratio, which increases the exposed surface area of the active component of the catalyst and enhances the contact between reactants and catalyst. Therefore, surface area plays an important role in the photocatalytic activity, and due to that, the focus has been shifted towards the semiconducting nanomaterials because of the high surface-to-volume ratio they possess. Semiconductor nanomaterials are one of the richest classes of nanomaterials. Usually in conductors, current is considered to flow due to electrons only, but here in semiconductor materials, it is caused by both electron and hole movements. The electronic properties and conductivity of semiconductors can be changed in a controlled manner by adding very small quantities of other materials called dopants [38, 39]. Nanoparticles that have a large band-gap semiconductor with unique structure and properties have been applied in photocatalysis, but the high energy requirement of UV radiation only limits their utilization for photocatalytic applications. Therefore, efforts have been made to improve the photocatalytic performance of nanoparticles in order to enhance the visible light absorption of semiconductor photocatalysts with improved stability.

Several modification techniques can be applied via different strategies, such as noble metal loading, ion doping, dye sensitization, addition of conjugated polymers to the structures, synthesis of nanorod arrays, one-dimensional nanorods, combination with other components, modification of metal oxide nanoparticles by non-metal doping, addition of transition metals,

use of binary and ternary semiconductors, etc., and among these doping techniques, doping is a more comfortable one compared to the other techniques [39, 40]. Doping is described as the intentional insertion of foreign elements into the empty crystal lattice of another element to change its properties. It is a standard method for improving nanoparticles' physical, chemical, optical, electrical, and biological characteristics [41].

2. 3. Metal Oxide Nanoparticles

Metal oxides represent the most diverse class of materials, with properties covering almost all aspects of materials science and physics. The improvement in the optical, electronical, magnetic, and chemical properties of these particles has originated from their nanoscale sizes. Metal oxide-supported metal particles have many potential applications in electronics, catalysis, gas sensing, and hydrogen storage [25].

In recent years, there has been an increasing interest in the synthesis of nanosized crystalline metal oxides because of their large surface areas, unusual adsorptive properties, surface defects, fast diffusivities, conductivity, ionic structure, freezing, melting, and color within the nanorange [18].

2. 3.1. Zinc Oxide Nanoparticles as Semiconductor and Doping Conditions

Transition metal oxides are a highly interesting group of materials because they possess a wide variety of structures and diverse electronic, magnetic, and optical properties [42]. Transition metals are defined as d-block elements as their atomic structures have incomplete d-orbitals in their electron configuration and, therefore, give rise to physical and chemical properties that differ from those of the main group elements. These elements are considered interesting for research as they retain multiple oxidation states caused by the proximity in energy of the d and ns shells. This provides a large number of configurations for their oxides, thus, widening the field of applications for transition metals [3]. Among the various types of nanomaterials, nanostructured transition metal oxides deserve special consideration for their outstanding properties and technological applications [14].

ZnO is a semiconductor with an n-type conductivity and a wide band gap of 3.37 eV. ZnO NPs are generally recognized as safe (GRAS) by the U.S. Food and Drug Administration (FDA, 21CFR182.8991) and are potentially applicable to treat infectious diseases. Because

of the unique properties that zinc oxide has, it is the best semiconductor compared to other oxides. When ZnO is irradiated, a pair of positive holes and electrons are generated in the valence band and conduction band. The secondary reactions of the positive hole and electron generate OH radicals. The OH radical, which is an influential oxidizer, reacts with organic pollutants and degrades them. The unique properties of ZnO NPs make viable and cost-effective surfaces suitable for different applications such as adsorbents, solar and fuel cells, catalytic agents, gas sensors, magnetic materials, hydrogen storage, photocatalytic degradation of organic dyes, pollutants from wastewater, and antimicrobial activity [14, 20–23].

As Adinaveen et al. [25] propose a comparison of different photocatalysts, the degradation activity of ZnO NPs under sunlight is highest, as shown in table 1 below.

Table 1. Comparison of Photocatalytic activity of ZnO NPs with different photocatalysts

Materials Used	**Biological Entity**	**Pollutant**	**Degradation efficiency (%)**	**Degradation time (min)**
ZnO	*Nepheliumlappaceum L*	Rhodamine B	96.3	180
NiO	*Nepheliumlappaceum L*	Tannery wastewater	83.99	120
TiO_2	*Jatrophacurcas L*	Methylene Orange	82.26	300
CuO	*Pyruspyrifolia*	Methylene blue	80.3	210
ZrO_2	*Ficusbenghalensis*	Methylene Orange	69	240
FeO	*Jatrophacurcas L*	Rhodamine B	67	180
CeO_2	*Maducha longifolia*	Methylene Orange	87	120

Pure ZnO has low photocatalytic properties with sunlight as the source of photon energy since sunlight only reaches about 4% of UV light/UV-A (k = 315–400 nm) and is dominated by 42–43% of visible light (k = 400–700 nm), which has lower energy. An efficient photocatalyst should absorb not only ultraviolet radiation but visible radiation as well because solar radiation is composed of 45% visible radiation and less than 10% ultraviolet radiation, in addition to other types of radiation. It may be useful to add further functionalities to ZnO rather than improve the pre-existing ones, with the final aim of designing a multifunctional system. ZnO also has a high rate of recombination between the electron (e^-) and hole (h^+),

reducing the chance of electrons being transferred to other molecules during photo induced redox reactions [43].

To overcome this constraint, much effort has been made to enhance the photocatalytic property of ZnO [6], including size reduction, facet engineering, photo-sensitization with dyes or quantum dots, decoration of the surface with charge separators, and by forming heterojunctions or composites with metal oxides or by impurity doping with several elements to induce electron delocalization and modify electron pathways in the presence of the new band of the doped atom. The dopant produces another band between the highest occupied molecular orbital (HOMO) and the lowest unoccupied molecular orbital (LUMO). In the photocatalyst concept, which usually uses inorganic compounds, the HOMO and LUMO are known as the valence band (VB) and conduction band (CB), respectively. The orbital of the modified atom usually occupies the space between VB and CB, which acts as an electron bridge to assist the electron excitation and slow down the recombination rate [44, 45].

For successful bulk modification by crystal doping, the dopant ions should fulfill some requirements. Firstly, the ionic radius of the dopant ions should be similar or nearly similar to that of Zn^{2+} [10]. Ions with a larger ionic radius are difficult to crystal dope, and doping of ions with a smaller or larger ionic radius will induce high lattice distortion, leading to the formation of physical defects that act as charge recombination sites for photo-generated electrons and holes, leading to decreased photocatalytic activities [11]. Secondly, in the case of doping a single element, ions with a valence number of two are preferred. If the dopant ions do not have the same valence number as zinc ions, the charge imbalance may result in enhanced recombination of photo-generated electrons and holes, so that doping may reduce photocatalytic activity. The efficiency of ZnO to absorb visible radiation can be enhanced by narrowing the band gap or dividing it into many subbands. The implantation of transition metal ions in the structure of ZnO is one of the techniques used for narrowing the band gap [1–3].

The implanting metals normally occupy the positions located between the VB and CB of ZnO. The photogenerated carriers are trapped, captured, and restricted at these localized positions by localized states of transition metal, and the recombination rate is decreased, which ultimately enhances the photocatalytic activity of ZnO [7–9].

The size quantization causes variations in the energy gap between the conduction band electrons and valence band holes, which result in changes in the optical properties of the doped metal oxide nanostructures [23]. Co/ZnO materials with a controllable band structure are particularly attractive because of the abundant electronic states of Co and the minor or negligible effect of Co on the structure of ZnO [12–16]. A decrease in ZnO particle size causes changes in the electrical, optical, and chemical properties; some authors believe that these changes are caused by the quantum confinement surface, thus enabling new applications. For instance, when the size of ZnO is reduced to the nanoscale, its activity against microorganisms is increased. Particularly in terms of antimicrobial applications, among the advantages of using an inorganic material rather than an organic material are reduced toxicity, improved durability, lower resistance, and good selectivity [24–27].

2. 4. Strategies for Nanoparticle Synthesis

The synthesis of nanoparticles can be carried out using different methods, broadly split between a top-down and a bottom-up approach. Top-down approaches, as the term suggests, are methods of synthesizing nanoparticles using bulk materials as the starting material, which is then broken down into desirable smaller forms [28]. On the other hand, bottom-up approaches "build" the nanoparticles using smaller molecules as the starting material or building blocks [28, 29].

The building blocks for the bottom-up synthesis of nanoparticles are atoms, molecules, and other particles that are miniature compared to the previous two [29]. The top-down approach is destructive, whereas the bottom-up approach is characterized by construction [28, 30].

Examples of the top-down approach include chemical etching, laser ablation, mechanical milling, electro-explosion, and sputtering. In these different methods, the bulk materials are first converted into powder form and then into particular NPs. Each synthesis method has its advantages and limitations. The top-down approach has many advantages, such as the production of the desired size and large quantity of nanoparticles, whereas the fabrication of NPs using this method leads to ecotoxicity, high energy consumption, and, on top of that, is expensive and time-consuming [2, 3].

The bottom-up approach is further divided into two classes: biological and non-biological approaches. Examples of non-biological approaches include titanium plate support synthesis,

flame spraying, spinning, laser pyrolysis, atomic condensation, and deposition of chemical vapors. These methods also use toxic chemicals and are expensive and time-consuming, whereas the biological approach uses various biotic resources such as plants, algae, microorganisms, and other biological molecules like starch, egg albumin, and gelatin for the production of different types of NPs. This biological approach is also known as the green approach [7–10]. This method is eco-friendly, simple, reliable, biocompatible, and easy for the synthesis of NPs. The synthesis methods of nanomaterials are shown in Fig. 2 below.

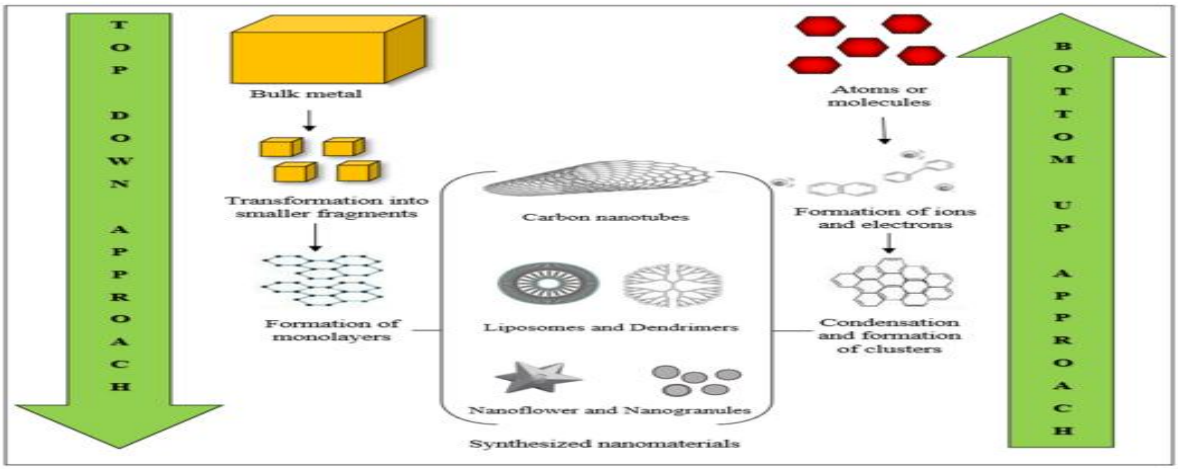

Fig 2. Schematic representation of major approaches involved in nanomaterial synthesis [11].

In contrast to bacteria, algae, and fungi, plants have been extensively used to synthesize metal oxide NPs. This is because of their abundance and safe nature, as well as the greater stabilization and reduction of plant phytocompounds [2].

The fabrication of nanoparticles from aqueous extracts of plant sources is a facile process that uses plant extract as a reducing agent and a metallic salt solution [35]. Plant-mediated nanoparticles depict a higher antimicrobial potential to combat infections in humans, which possess bacterial and fungal etiologies [36].

2. 4.1. Green synthesis

Green protocols for the synthesis of nanoparticles have been attracting a lot of attention because they are ecofriendly, rapid (robust), and cost-effective. Likewise, NPs synthesized by using green chemistry have no or little cytotoxicity as compared to chemically synthesized NPs [42](Fig.3).

It is now well established that various organic components present in plant tissues are capable of acting as effective biological factories to significantly reduce eco-friendly contamination, and can recover metals from industrialized waste. Moreover, mixtures of molecules identified in plant extracts can act as both stabilizing (capping) and reducing agents all through NP synthesis [46, 47].

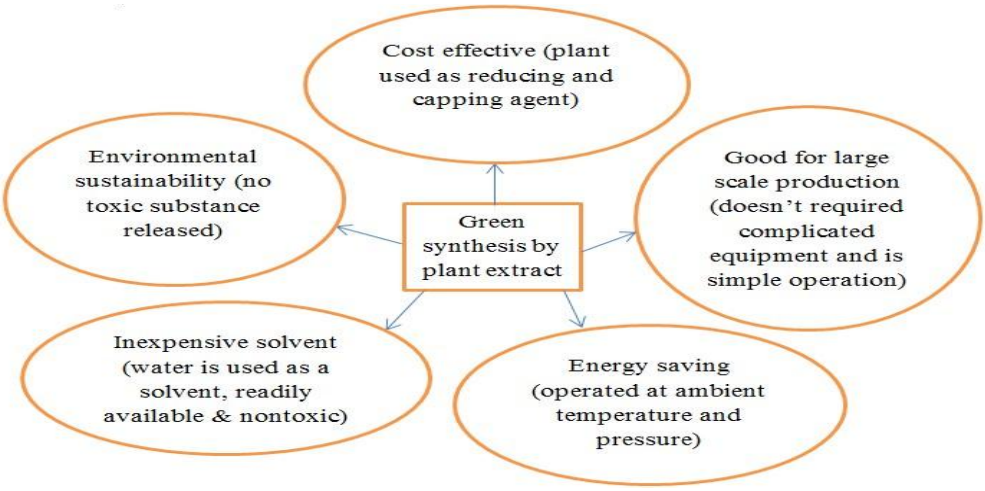

Fig 3. Benefits of bio-derived fabrication or green synthesis of nanoparticles over chemical and physical procedures [2].

A. Mechanism of Green Synthesis

The secondary metabolites of plants are responsible for the reduction of metal ions into metal atoms. Metal salts like nitrates, chlorides, oxides, and sulfates have a high reduction potential due to the attachment of metal to the chloride, oxide, and sulfide parts and their tendency to donate electrons. As a result of both of these issues, the electronic density of the conjugative salts of metal increases. So metals in their ionic form can easily get detached from their anionic part and get reduced into stable form by using plant extract [48, 49]. The secondary metabolites of plants, including alkaloids, flavonoids, polyphenols, and terpenoids, act as chelators for metal

ions and reduce them to zerovalent states. Mostly the OH group of polyphenols and flavonoids develops coordination with metal ions. We can describe the mechanism of plant-mediated synthesis of metal and metal oxide NPs by considering the following three phases: The activation phase involves the reduction of metal ions, and reduced metal atoms undergo nucleation; the growth phase involves the spontaneous coalescence of small adjacent NPs into larger NPs, that is, Ostwald ripening (a process in which NPs are directly formed through heterogeneous nucleation and growth and further reduction of metal ions); this process enhances the thermodynamic stability of NPs; The termination phase decides the final shape of NPs. In the case of metal oxide NPs, the end product is air dried or calcined in air to get the final metal oxide NPs. The nature and concentration of the plant extract, pH, temperature, metal salt concentration, and contact time are known factors affecting the green synthesis of NPs [15–19].

2. 5. Characterization techniques for metal oxide nanoparticles and metal-doped metal oxide nanocomposite

UV-Vis spectroscopy uses light in the visible range. The principle of UV-vis spectroscopy is based on the absorption of ultraviolet light or visible light by chemical compounds, which results in the production of distinct electronic spectra. UV-Vis spectroscopy was used to show the band gap energy of synthesized nanoparticles. The band gap increases with decreasing particle size, and the absorption edges are shifted to higher energy (blue shift) with decreasing particle size [42].

The plots of variation of $(\alpha h\nu)^2$ versus $h\nu$ for the ZnO and Co-ZnO NCs were presented. These plots are known as Tauc's plots, and they are used to find out the accurate optical band gap value by the extrapolation of the linear part, which is used to calculate an optical band gap of the nanoparticles. The tauc plot has the photon energy ($h\nu$) on the X-axis and a quantity $(\alpha h\nu)^2$ on the Y-axis, and extrapolating the linear portion of the curve to the X-axis yields the band gap energy of the material [42].

FT-IR spectroscopy analysis is a method based on the principle of infrared spectroscopy. Functional groups can be associated with characteristic infrared absorption bands, which correspond to the fundamental vibrations of the functional groups [44]. FT-IR is very useful to study surface chemistry and identify possible biomolecules for the capping and stabilization of

nanoparticles. The possible functional groups that are present in the plant extract and synthesized nanomaterials were identified in the range of 4000-400 cm^{-1} [32, 42].

For phase identification, XRD patterns were collected on an X-ray diffractometer. The atomic planes of a crystal cause an incident beam of X-rays to interfere with one another as they leave the crystal. XRD is a non-destructive technique used to identify crystalline phases and orientations, measure the thickness of thin films and multi-layers, and determine the atomic arrangement and structure of the NPs. The XRD technique is also used to get information like lattice parameters, the crystallite size of crystals, defects, and strains, and the average crystallite size of the nanoparticles, which was calculated using Scherer's formula [50, 45].

$$D = \frac{\kappa\lambda}{\beta \cos\theta} \quad \text{.....1}$$

Where D is grain size, K is an empirical constant of 0.9, is the wavelength of the incidence beam (λ=1.5406 Å), β is the full-width half maximum (FWHM) in radian, and θ is the angular of the peak position. The scanning electron microscope is a very useful instrument to get information about topography, morphology, and composition information of the sample [42]. The morphologies of the phytomolecules coated ZnO nanoparticles [37] and Co-ZnO nanostructures were studied using SEM [25, 42].The SEM instrument is based on the principle that the primary electrons released from the source provide energy to the atomic electrons of the specimen, which can then release secondary electrons (SEs) and an image can be formed by collecting these secondary electrons from each point of the specimen [49].

2.6. Dyes, their sources, and removal mechanisms.

Dyes are colored compounds that are widely used in textiles, printing, rubber, cosmetics, plastics, and leather industries to color their products, generating a large amount of colored wastewater. Dyes are chemical compounds that attach themselves to textiles or surface shells to impart color. These dyes are highly toxic and even carcinogenic to microbial populations and mammalian animals; hence, they are needed to be removed from the water effluents before they are released into water bodies. Dyes are stable to light and not biologically degradable; they are resistant to aerobic digestion and signify one of the hard groups to be removed from industrial wastewater [51].

Fig 4. Pollutants and affected water bodies by synthetic organic dyes [52]

There are many conventional methods available to remove dyes from industrial wastewater (effluents). These include biological treatment, electrodialysis, ozonation, coagulation/flocculation, adsorption on a solid phase, membrane separation, electrochemical oxidation, ultrafiltration, sorption-floatation, etc. However, these methods have several limitations, like: biological treatment methods involve a long reaction time and emit bad odors; incineration can produce toxic volatile gases; ozonation presents a short half-life (20 min); and the stability of ozone is strongly affected by the presence of pH, salts, and temperature. It is expensive, ineffective, and results in high levels of sludge and by-products [12].

The photocatalysis process can degrade toxic organic pollutants into less toxic by-products through mineralization, ensuring zero waste production [53].

2.6.1. Photocatalytic Activity

Photocatalysis is the amalgamation of photochemistry and catalysis. The word "photocatalysis" is derived from the Greek language and composed of two parts:

The prefix photo means light. Catalysis is the process where a substance alters the rate of a chemical transformation of the reactants without being altered in the end. The substance, which is known to be a catalyst, increases the rate of the reaction by reducing the activation energy. Hence, photocatalysis is a process where light and catalysts are concurrently used to support or speed up a chemical reaction.

The noteworthy features of these processes include undisposed waste and cost-effectiveness when sunlight, near-UV light, or visible light can be used as a source of irradiation. Photocatalyst is a term that means photon assisted generation of catalytically active species. In general, photocatalysis can be defined as "a change in the rate of chemical reactions or their generation under the action of light in the presence of substances called photocatalysts that absorb light quanta and are involved in the chemical transformations of the reactants" [26].

2.6.2. Photocatalytic mechanism

A photocatalytic reaction primarily depends on wavelength, or light (photon) energy, and the catalyst. In general, semiconducting materials are used as catalysts that act as sensitizers for the irradiation of light stimulated redox processes due to their electronic structure, which is characterized by a filled valence band and a vacant conduction band [54]. Heterogeneous photocatalysts have been widely used for the degradation of organic pollutants recently. Besides, this technology can also be efficient in destroying pathogens such as viruses, bacteria, and so on in water effluents [37].

The semiconductor photocatalysts have advantages such as low manufacturing cost, non-toxicity, a high surface area and a high amount of active sites, simple preparation for large scale applications, a short charge diffusion distance, which is important to decrease bulk charge recombination, and tunable properties when modified with dopants, sensitizers, etc. [49]. Besides, with the photocatalytic technique, complete degradation of pollutants can be achieved so that the method does not leave a trace amount of pollutants [39].

However, the removal of catalyst from the reaction medium, serious surface charge recombination, and poor chemical stability due to the large surface area can be serious problems for such systems. In order to obtain better photocatalytic activity, a semiconductor with a lower band gap energy should be chosen. Besides, cost, easy production, stability in the reaction medium, being eco-friendly, and effectiveness are the crucial parameters that should be considered for the selection of a photocatalyst [29].

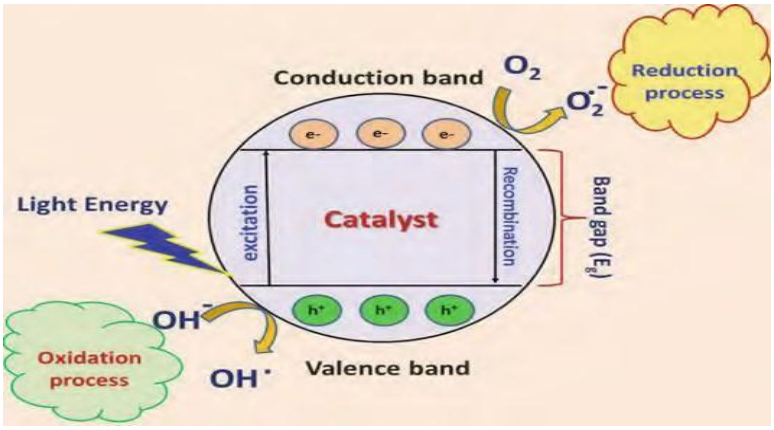

Fig 5. Shows the schematic representation of semiconductor photo-catalytic mechanism [55].

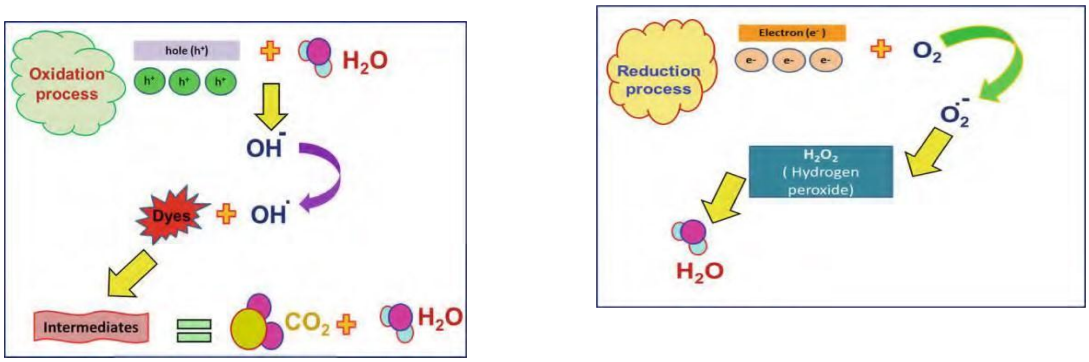

A B

Fig 6. Schematic representation of a) oxidation and (b) reduction mechanism [55].

The different mechanisms for the Photocatalytic activities of pure zinc oxide NPs have been proposed as the following.

$$ZnO^{2+} + hv \rightarrow e^- + h^+$$

$$ZnO^{2+} + e^- \rightarrow ZnO^{2+}$$

$$ZnO^{2+} + O_2 \rightarrow Zn + \bullet O_2$$

$$h^+ + H_2O \rightarrow \bullet OH + H^+$$

$$Dye + \bullet O_2 \rightarrow No\ Dye$$

$$Dye + \bullet OH \rightarrow No\ Dye$$

Fig 7. Scheme for dye degradation [36].

2.6.3. Parameters Affecting Photocatalysis

The rate of photomineralization of an organic compound by the photocatalysis method primarily depends on the following parameters: structure, shape, size, and surface area of the catalyst; reaction temperature; pH; light intensity; amount of catalyst; and concentration of wastewater [56–58]. Nowadays, besides the development of multidrug-resistant microorganisms, which is creating a very challenging issue all over the world, the disposal of colored synthetic organic waste water from different industries causes serious problems to the aquatic ecosystem. Because of this, the aquatic environment is contaminated, which poses a serious threat to living organisms. Therefore, it is highly desirable to develop a simple but effective way to degrade these colored organic wastes as well as kill or inhibit microbial growth. Pharmaceutically, antibiotics were applied to microorganisms, but successful reduction was not obtained due to adaptations of these microorganisms to the drug. Also, conventionally, a biological treatment or degradation process is utilized to decolorize the dyes, but it is ineffective for the complete removal and degradation of dyes. Photocatalytic degradation by NPs in wastewater treatment has numerous advantages over the physical, chemical, and biological methods available to date. These include: rapid oxidation, no formation of polycyclic products, and oxidation of pollutants (up to the PPb level), chemical stability, optical and electrical properties, and an effective, inexpensive, and eco-friendly method [59, 60]. Literature studies have demonstrated that nanocomposites are more effective photocatalysts for the degradation of dyes; combinations of two individual metals/or their oxides may be more efficient than either individual [47]. Among different methods, photocatalysis using NPs as an alternative to physical, chemical, and biological methods shows great potential. In the last few years, the catalytic process derived from solar energy or other radiation energy has been studied for the successful degradation of harmful organic dyes into environmentally friendly materials. Recently, nanomaterials have been effectively used as active catalysts for the degradation or oxidation of organic dyes. The photocatalytic degradation occurs due to the effective separation of excited electrons in the conduction band (CB) and holes in the valance band (VB) under light illumination, which could be captured by some surface species in the surroundings, such as hydroxyl or O_2 groups [35].

2. 7. *Allium cepa L*. plant

Allium cepa L. (the common red onion) belongs to the *Allium* genus from the Amaryllidaceous family and is recorded in around 918 species around the world. Only one bulb is produced by each onion plant, therefore, the "onion" word originated from the "unio" word, which refers to "one", "single" in Latin [20]. Among the vegetables rich in bioactive compounds, *Allium cepa L* is one of the oldest plants cultivated around the world and consumed as a vegetable and spice. It is greatly appreciated as a medicinal plant in traditional medicine for its high content of phytochemicals, including polyphenols, flavonoids, and sulfur-based compounds [27]. It is the second most important horticultural crop after tomatoes, with a worldwide current production that makes its related by-products widespread and easily available. Furthermore, onion waste is an easy handling biomass because of its low weight and dryness [21].

Various reports have already been published in the literature that show that nanomaterials such as nanoparticles and nanocomposites are effective candidates for the photocatalytic degradation of synthetic organic dyes and toxic chemicals and the inhibition of microorganisms [37]. In this thesis, we have synthesized ZnO Nps and Co/ZnO NCs through the green route using red onion skin aqueous extract for the first time and utilized them as efficient photocatalysts for the degradation of the hazardous Methylene Blue dye under natural sunlight irradiation and antimicrobial tests on two gram positive bacteria, one gram negative bacteria, and one fungal strain at room temperature. The synthesized nanoparticles and nanocomposites were characterized by XRD, SEM, UV-Vis, and FT-IR spectroscopy.

3. MATERIALS AND METHODS

3.1. Chemicals and reagents

All chemicals and reagents used in this study were of analytical grade and used without further purification. Zinc (II) nitrate hexahydrate, Zn $(NO_3)_2$.$6H_2O$, (99.5%), Alpha Chemica, India; Cobalt (II) nitrate hexahydrate,$Co(NO_3)_2.6H_2O$ (99.8%, Alpha Chemica, India), Sodium Hydroxide, NaOH (99%, Sigma - Aldrich, UK), Ethanol (99. 9% Ranchem Industry, Turkey), Methylene Blue (Merck, Dermstadt, Germany), Hydrochloric acid, HCL (38%, Merkel, Germany), Sodium Chloride, NaCl (99. Loughbrough, LE 115RG, UK), distilled water, absolute ethanol (99.9 %) ,filter paper (Whatman No. 1 and 4, *Allium cepa* plant peel) were used.

3.2. Apparatus, equipment, and scientific instruments

Oven (model: 158005/12, Gallen Kamp, England), Mortar and pestle, digital balance (Adam, AFP-110L, UK), Magnetic stirrer plate (Staffordshire ST15-OSA, UK), refrigerator (BekoRRN2650, Turkey), centrifuge (Table Top Centrifuge, PLC-02; Taiwan), centrifuge tubes, beakers, test tubes, droplets, graduated cylinders, rack, cuvettes, eryemer flasks, electrical grinder, reagent bottles, and volumetric flasks.

Double beam UV-Vis Spectrophotometry (UV-Vis: SPECORD 200 PLUS -223, Germany), single-beam UV-VVis Spectrophotometry (JENWAY - 6705), pH/Conductivity Meter (Bante 902P, China), X-Ray Diffractometer (XRD-700 Drawell, Artist of Science, Shimdazu, USA), Fourier Transform Infrared Spectroscopy (FT-IR:Perkins Elmer, Spectrum Two LITA, L1600300, UK), and Scanning Electron Microscopy (SEM,JCM-6000Plus machine) were used during the study.

3.3. Sample collection and preparation

The *Allium cepa L*. plant peel was collected around the Jimma University cafeteria from Jimma Zone, Jimma, and Southwest Ethiopia and transported to Jimma University chemistry research laboratory. And then, after, thoroughly cleaning with tap water to remove debris and other contaminants, followed by distilled water and shade drying at room temperature. The well dried sample was ground with a mortar and pestle, and then the aqueous extract of the peel powder was prepared by boiling 10 g of the powder with 100 mL of distilled water in a 250 mL beaker at about 60 °C and stirring for 20 minutes [61]. And the reddish extract was cooled to room temperature and further centrifuged at 400 rpm for about 10 min to remove any heavy insoluble

biomaterials. The supernatant was collected and finally, the extract was kept in a refrigerator to be used for further experiments [62].

3.4. Phytochemical tests of *Allium cepa L*. plant peel extract

3.4.1. Test for flavonoids

Alkaline reagent Test: 1 mL of the extract was treated with 5 mL of NaOH. The presence of flavonoids is confirmed by the formation of the intense yellow color [63].

3.4.2. Test for alkaloids

Wagner's Test: 1 mL of the solvent extract was acidified with 1 mL of 1.5% v/v HCl, and 1 mL of Wagner's reagent was added. The occurrence of alkaloids is indicated by the formation of yellow and/or brown precipitates [23].

3.4.3. Test for saponins

Frothing Test: About 1 mL of the extract was diluted separately with 20 mL of distilled water and shaken in a graduated cylinder for 15 minutes. A 1 cm layer of foam was formed, which indicates the presence of saponins [12].

3.4.4. Test for tannins and phenolic compounds

Ferric chloride test: 1 mL of the extract was treated with a few mL of 5% neutral ferric chloride. The formation of a dark blue and/or bluish-black color product showed the presence of tannins and phenols [12, 42].

3. 5. Parameter optimizations for the synthesis of ZnO NPs and Co/ZnO NCs

The different parameters that are expected to affect the synthesis of NPs and NCs were studied by analyzing the samples through the UV-Vis spectrum by varying one parameter and keeping the others constant.

The reaction time is essential for the synthesis of NPs and NCs [4]. The effect of reaction time was studied during the green synthesis of Co/ZnO NCs for every 1 h difference for 3 h.

The presence of OH- in an alkaline pH environment might enhance the reducing and templating/chelating capabilities of the biomecules in the peel extract due to the better accessibility of the functional groups present in the extract for nucleation at alkaline pH [38]. The green synthesis of Co/ZnO NCs using an aqueous extract of red onion peel was examined at different pH values of 6, 8, 9 and 10 by keeping other parameters constant.

Temperature is one of the major factors that significantly influence the shape, size, stability, and yield of NCs synthesized via the green route. In most cases, the synthesis of NPs using green technology requires temperatures less than 100 °C or ambient temperature [41]. The effect of temperature on the green synthesis of Co/ZnO NCs was studied by varying it at 25, 45, 65, and 85 ^{o} C by keeping all other parameters constant.

The synthesis of Co/ZnO NCs using plant extract is mainly influenced by the types of biomolecules found in the plant extract and the volume used. The volume of plant extract used in the synthesis of NMs plays a significant role in the reduction of metal ions into reduced metal atoms [15]. To get the optimum amount of plant extract for reduction of Zn^{2+} and Co^{2+} ions, the volume optimization of red onion peel aqueous extract was studied with different volumes of red onion peel aqueous extract (10, 15, and 20 mL) at fixed values of other factors.

Formation of Co/ZnO NCs was also investigated by varying Zn $(NO_3)_2$.$6H_2O$ solution from 0.05, 0.1, and 0.15 M by keeping plant extract volume, dopant concentration, reaction time, and temperature constant.

The absorption peak of Co/ZnO NCs could also be affected by the concentration of dopant [23]. To see the effect of dopant (Co) concentration on the absorption peak of ZnO NPs, the dopant concentrations were studied at different concentrations (0.01 M (1%)), 0.05 M (5%), and 0.1 M (10%)) at fixed amounts of other parameters.

3.6. Synthesis of Zinc Oxide Nanoparticles

The synthesis was performed according to [15] with slight modifications. Bio-fabrication of ZnO NPs was initiated by taking 0.15 M of an aqueous Zinc (II) nitrate hexahydrate, $Zn(NO_3)_2$.$6H_2O$ solution, in a 250 mL conical flask, followed by continuous stirring at 65 ◦C for 10 min. The aqueous extract of *Allium cepa L.* (20 mL) was added to the Zn $(NO_3)_2$.$6H_2O$ solution, and the reaction mixture was constantly stirred at the same temperature to assist the electrostatic interaction of Zn^{2+} with the biomolecules present in the aqueous peel extract, The color of the experimental mixture turned light reddish to yellowish as the phytochemicals of the extract capped the Zn^{2+} ions and initiated the nucleation of ZnO NPs. As the nucleation persisted, the phytochemical moieties stabilized the process, and the system reached equilibrium within a short time at a low pH (3). Solution pH from low to high enhanced the nucleation, and phytochemical moieties stabilized the ZnO NPs [48–51]. In Step II, the reaction mixture (pH = 8) was maintained by adding dropwise a freshly prepared NaOH (2.0 M) solution, under continuous

stirring at 65 ◦C. The light white precipitation occurred under constant stirring of the reaction mixture for the next 2 h at 65 ◦C, which indicated the formation of ZnO NPs [36–38]. The final product was cooled and then collected by centrifugation of the reaction mixture at 400 rpm for 20 min. The precipitate was washed several times with distilled water and ethanol to remove any additional impurities or unreacted materials from the surface of the biosynthesized material. In the final step III, the synthesized material was kept in an oven at 60◦C for 1 h, followed by a crucible dish for an additional 2 h at room temperature to achieve complete dryness.

3.6. 1. Synthesis of cobalt-doped zinc oxide nanocomposites

To synthesize Co/ZnO NCs according to [15, 17] with slight modification, 0.15 M of Zinc (II) nitrate hexahydrate, ($Zn(NO_3)_2$.$6H_2O$) was stirred for 20 min, followed by 20 mL of peel extract dropwise, followed by 30 mL of 5% Cobalt (II) nitrate hexahydrate, $Co(NO_3)_2.6H_2O$. The mixture was progressively stirred for 20 minutes at room temperature, and a reddish to yellowish color was observed. To adjust the pH of the solution, freshly prepared 2 M NaOH was added drop by drop to bring the pH to 8. The resultant product was stirred at room temperature for 2 hours. Subsequently, the obtained solid was cooled and then collected by centrifugation of the reaction mixture at 400 rpm for 20 min. The precipitate was washed several times with distilled water and ethanol to remove any additional impurities or unreacted materials from the surface of the biosynthesized material. In the final step III, the synthesized material was kept in an oven at 60 °C for 1 h, followed by a crucible dish for an additional 2 h at room temperature to achieve complete dryness.

3.7. Methods of Characterization

3.7.1. UV-Vis, FT-IR, XRD, and SEM Analysis

The electronic spectra of the ZnO NPs and Co/ZnO NCs in solution were run in the range of 300–800 nm on a 6705 UV/Vis spectrophotometer (JENWAY).

The electronic spectra of the ZnO NPs and Co/ZnO NCs in solution were run in the range of 300–800 nm on a 6705 UV/Vis spectrophotometer (JENWAY). The principle of UV-Vis spectroscopy is based on the absorption of ultraviolet light or visible light by chemical compounds, which results in the production of distinct spectra through diluting the samples during analysis.

Fourier transform infrared (FT-IR) spectra recorded in 4000-400 cm^{-1} were used to identify the presence of functional groups and to receive valuable information regarding the presence of ligand in the metal NPs as KBr discs on a Perkin Elmer. The FT-IR technique is used to obtain an infrared spectrum of the absorption/emission of solids and gather spectral data in an extensive spectral range.

The crystallinity and crystalline phase of synthesized samples were determined through X-ray diffraction (XRD) profiles (DR AWELL XRD-700 using 2CuKα radiation) in 2θ range of 20° to 80° with a scan speed of 0.03°/min. XRD patterns are collected on an X-ray diffractometer. These X-rays are generated by a cathode ray tube, filtered to produce monochromatic radiation, collimated to concentrate, and directed toward the sample [45]. The atomic planes of a crystal cause an incident beam of X-rays to interfere with one another as they leave the crystal. The morphological features of the prepared ZnO NPs and Co/ZnO nanostructures were studied using scanning electron microscopy (JCM-6000Plus machine). The sample was simply deposited onto the top of an adhesive fastened to an aluminum stub/holder. Most often, conductive carbon tape is used to sequester the sample. Computer software was used to collect/analyze the resulting patterns to determine the crystallography of the material. The SEM instrument is based on the principle that the primary electrons released from the source provide energy to the atomic electrons of the specimen, which can then release secondary electrons (SEs), and an image can be formed by collecting these secondary electrons from each point of the specimen [49].

Fourier transform infrared (FT-IR) spectra recorded in 4000-400 cm^{-1} was used to identify the presence of functional groups and to receive valuable information regarding the presence of ligand in the metal NPs as KBr discs on a Perkin Elmer. The FT-IR technique is used to obtain an infrared spectrum of the the the th or the the absorption/emission of solids and gather spectral data in an extensive spectral range [64].

The crystallinity and crystalline phase of synthesized samples were determined through X-ray diffraction (XRD) profiles (DR AWELL XRD-700 using 2CuKα radiation) in 2θ range of 20° to 80° with a scan speed of 0.03°/min. The morphological features of the prepared ZnO NPs and Co/ZnO nanostructures were studied using scanning electron microscopy (JCM-6000Plus machine). The energy band gap of ZnO NPs and Co/ZnO NCs was determined using the tauc relation. The tauc plot is a convenient way of studying the optical absorption spectra of a

material. It has the photon energy (hv) on the X axis and $(\alpha h\nu)^2$ on the Y axis, and extrapolating the linear portion of the curve to the X axis yields the band gap energy of the material [65].

3.8. Applications of synthesized NPs and NCs.

3.8.1. Optimizations of parameters for the degradation of methyl blue dye.

A. Catalyst dosage.

The number of organic pollutants adsorbed on the surface of NPs is a crucial factor that influences their photocatalytic performance. In this study, a catalyst dosage was varied from 30 to 70 mg at constant pH, initial dye concentration, and time to see its effect on the decolorization efficiency. Equilibration in the dark is required because it is assumed that photocatalytic reactions of organic pollutants occur in the adsorbed phase [21]. Dark equilibration was performed 30 minutes before illumination in the sunlight. The intensity condition was checked by UV-Vis spectroscopy measurements.

B. Effect of pH

I. Determinations of the point of zero charge.

Determining the pH at point of zero charge (pHpzc) is a substantial step in predicting the charge on the nanoparticle surface during the photocatalytic degradation process.

The pHpzc was carried out according to [15, 66] and accordingly, 0.1 M (0.58 g) of NaCL in 100 mL distilled water was prepared and added to different five 50 mL round bottom flasks, followed by the addition of 50 mg of Co/ZnO NCs to each flask, and the pH_i for each was adjusted to (2, 4, 6, 8, and 10) (appendix 1A) by using 0.1 M of HCl and NaOH. The flas were shaken in a shaking water bath for 24 at room temperature, and then after that, the pH_f of each was recorded, and finally the pH, or ($pH_f - pH_i$) was calculated and drawn againist pH_i. The value of pHpzc of Co/ZnO NCs was determined from the points where the initial pH equals the final pH. Adsorption of MB on the surface of Co/ZnO NCs was evaluated after 30 minutes of stirring the solution in the dark at different pH values of 8, 9, and 10. The pH of the MB dye was adjusted by 0.1 M of NaOH, and the percentage degradation was determined by measuring absorbance and calculating the percentage degradations at different time intervals from 15 to 60 min.

C. Effect of initial dye concentration

The concentration of dye is one of the main parameters that affect the degradation efficiency of photocatalytic degradation [40]. The effect of the initial dye concentration on the decolorization

of MB was studied under natural sunlight irradiation by varying the initial MB dye concentration from 10 mg/L to 30 mg/L at a fixed time, pH, and nanocatalyst dose to see its effect on degradation efficiency after 30 minutes of stirring the solution in the dark.

D. Effect of irradiation time.

UV-Vis absorbance spectra were investigated to show the impact of irradiation time on the MB dye, and intensity was checked at different time intervals from 15 to 60 min by keeping the initial MB dye concentration, pH, and nanocatalyst dose constant to see their effect on degradation efficiency after a dark equilibration test for 30 min.

After the optimization process was completed, the photocatalytic experiment on demineralizations of MB dye was investigated according to [13, 15, 66] with some modifications. To evaluate the photocatalytic performance of the prepared samples towards the degradation of MB dye, 50 mg of the prepared samples (ZnO nanoparticles or Co/ZnO nanocomposites) was dispersed in 100 mL of 10 ppm or 10 mg/L MB dye solution in glass vials, which were used as the reactors, and thoroughly mixed and kept in the dark for 30 minutes to reach the adsorption-desorption equilibrium between the photocatalysts' surface and dye solution. The reaction suspensions containing MB and nanostructured ZnO and Co/ZnO photocatalysts were irradiated with sunlight for 60 minutes with intermittent (continuous) shaking for uniform mixing of the photocatalysts with the MB dye solutions. These experiments were carried out at midday (between 6.00 and 7.00 AM) during the peak winter season, ensuring irradiation with sunlight of maximum luminosity. Then aliquots (suspensions) of 5 mL were collected at regular intervals of time and centrifuged (10,000 rpm for 5 min) at different definite time intervals to separate the bio-fabricated ZnO NPs or Co/ZnO NCs from the suspensions. Concentrations of the MB dye in the resultant solutions were monitored by UV-visible absorption spectroscopy in the wavelength range of 200–800 nm, with distilled water as the reference medium, and absorbance intensity depletions were measured at a maximum wavelength of 665 nm in the indicated wavelength range . The photocatalytic efficiency of the photocatalysts for the degradation of the MB dye was calculated using the following formula :

%degradation = $[(A_0 - A_t)/ A_0] \times 100 = C_o - C_t / C_o \times 100$..... (2).

Where C_o is the initial concentration and C is the final concentration at time t while A_0 is the initial absorbance of dye and A_t is absorbance of dye at any time t of the MB dye sample with bio-fabricated ZnO NPs or Co/ZnO NCs) .

3. 8.2 Reusability performance of the nanoparticles and nanocomposites

The recycilibity of the NCs was performed according to [15], and accordingly, the optimized (50 mg) Co-ZnO NCs were separated from the supernatant solution by centrifuging and then washed, dried, and reused three times (three times) at optimized 60 min and pH 9 to compare the degradation efficiency with the original nanocatalysts. The degradation efficiency of ZnO NPs was checked by the same procedure at these optimized variables and compared with that of Co/ZnO NCs.

3.8.3 Antibacterial and Antifungal Activities.

The study on antimicrobial activity Plant extracts, NPs and NCs synthesized were carried out using the agar disc diffusion method. Zones of inhibition were measured in millimeters (mm) as a diameter in areas where no growth inhibition of the bacteria was visible. Bacterial suspension (1. 0×10^8 CFU/ mL) was then inoculated to standard petri dishes, which were formerly prepared using Muller-Hinton Agar according to manufacturer's procedure. The tests were performed in duplicate. Small volumes of bacterial suspensions were swabbed to each MHA plate and then evenly seeded and streaked by means of two or more times, rotating the plate approximately 60° each time to ensure an even distribution of inoculums, and finally the rim of the agar was swabbed. Test solutions were prepared by dissolving 250 mg of NPs and NCs into 1 mL of DMSO to get final concentration of 100 mg/L. Sterile filter paper discs (6 mm) were soaked with a stock solution of extracts and then placed over the seeded NMs at equidistance. The plates were then inverted and incubated at 37 ^{o}C for 24 h. The bioassay for antifungal activities was the same procedure described for bacterial activities. For each bacterial and fungal strain, the standard gentamicin and clotrimazole were taken, respectively, as positive controls and DMSO as a negative control for the test experiment at room temperature.

A. Minimum inhibitory concentration (MIC).

MIC is defined as the lowest concentration of the antimicrobial agent that inhibits microbial growth after 24 h incubation. The most effective NPs and NCs exhibiting strong antibacterial activity at 100 mg were manipulated to determine their MIC using the agar disc diffusion method

and evaluate their efficiency. Different concentrations of the NPs and NCs (100, 75, 50, and 25 mg/L) were prepared by the serial two-fold dilution method separately by dissolving 100 mg in 1 mL acetone, sterilizing through a Millipore filter, and loading their requisite amounts over sterilized filter paper discs (6 mm in diameter). Muller-Hinton agar was poured into sterile petri dishes and seeded with bacterial suspensions of the pathogenic strains. The loaded filter paper discs of the effective NPs were placed on top of the Muller-Hinton agar plates and then incubated at 37 ^{o}C for 24 h. The inhibition zones were measured by ruler and recorded against the concentrations of the effective, NPs, NCs, and plant extracts.

4. RESULTS AND DISCUSION

4. 1. Phytochemical screening of the red onion peel plant extract

During this study, phytochemical tests were conducted to identify classes of secondary metabolites present in the peel-aqueous extract of red onion. The primary phytochemical screening of the extract showed the existence of phenolics (with very intense color), flavonoids, alkaloids, and tannins with intense color, as shown in Table 2 below.

Table 2. Phytochemical components of *Allium cepa L.* peel extract

S/No	Phytochemical	chemical tests	results
1	Phenolics	ferric chloride	+ ++
2	Saponins	frothing test	+
3	tannins	ferric chloride	++
4	flavonoids	alkaline reagent	+
5	alkaloids	Wagner`s test	+

+ indicates the presence of phytochemicals, whereas ++ and +++ indicate high and higher intensity, respectively.

These phytochemicals, especially phenolics and tannins, act as capping and stabilizing agents for the synthesis of nonmaterials. This result is in good agreement with the literature [21], in which it was tested for the presence of phytochemicals in the red onion peel extract by ethanol solvent. However, according to [21], tannins were not present in the extract, in contrast to this investigation. This may be due to the type of solvent used during extraction, since different solvents can extract different families of phytochemicals based on their polarity, varying the biological activity of the extracts.

4.2. Parameter optimizations for the synthesis of Co/ZnO NPs and Co/ZnO NCs

4.2.1. Effect of reaction time

The UV-Vis analysis of the samples displayed a small intensity peak at 1 h, and the intensity band increased and a sharp peak with maximum wave length (369 nm))was formed as the time progressed to 2 h (Fig. 8). This indicated enhanced nucleation rate and formation of small sized NCs, and by increasing further to 3 h, a decrease in lower wave length nearly similar to that of 1

h was observed, so 2 h was taken as the optimum reaction time for biosynthesis of Co/ZnO NCs. Therefore, literature [5] found a similar result to this finding and concluded that increasing the reaction time increases the rate of reduction of metal ions until the reaction reaches completion. But, according to literature [66, 67], as contact time increases, the overall concentration of the nanomaterial increases until equilibrium is reached, and a longer reaction time causes an increase in size and also enhances the agglomeration of the nanocomposite rather than nuclei formation [45].

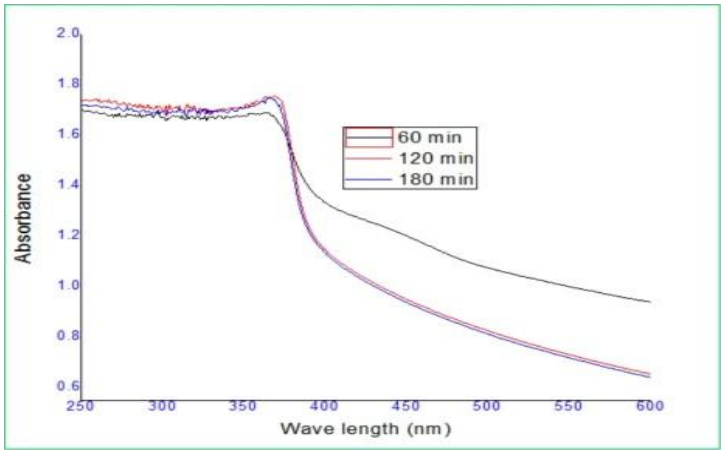

Fig 8. UV-Vis spectra of time optimization

4.2.2. Effect of pH

Out of the optimized pH, pH 8 was taken as the optimum to synthesize NCs because it gave a sharp peak at maximum wave length (365 nm), as seen from Fig. 9 below, and this result was in close agreement with the recently reported literature [5], which studied the antibacterial activity of red onion skin ethanol extract supported ZnO NPs and showed pH 8 as the optimum condition for synthesis.

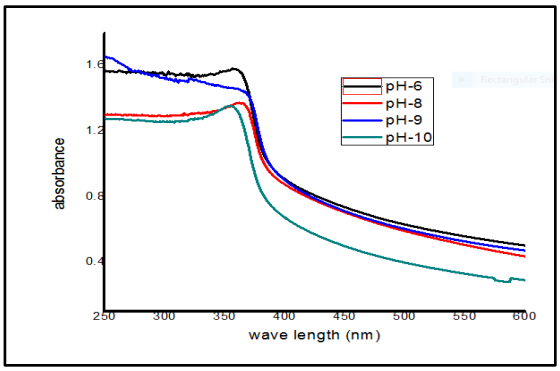

Fig 9.UV-Vis spectra of pH optimization.

4.2.3. Effect of temperature

At 25 ^{o}C, the Co/ZnO NCs showed a small absorption peak, indicating that no adequate Co/ZnO NCs were formed [68] (fig. 10). As the temperature increased from 45 to 65 ^{o}C , the intensity of the peak increased, and especially at 65 ^{o}C a sharp peak with a wave length of 362 nm was formed. This may be related to increasing reaction temperature, which improves the reaction rate up to the optimum condition for enhancement of nucleation rate. Even though there was a shift in wave length at 85 ^{o}C , a sharp peak didn't form. Therefore, 65 ^{o}C was taken as an optimum condition to biosynthesize Co/ZnO NCs.

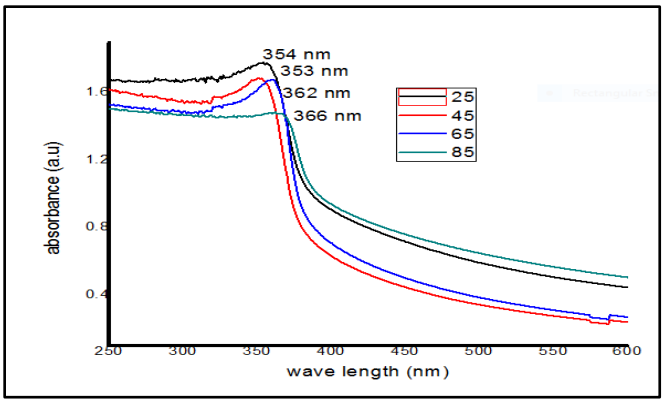

Fig 10. UV-Vis spectra of temperature optimization

4.2.4. Plant extract optimization

A red shift in the lambda from 360 to 362 nm was observed (Fig. 11) when the volume of the extract was increased from 10 to 20 mL, and the peak formed was also sharp [63]. This was attributed to the phytochemicals present in the plant extract, which are responsible for the bioreduction and stabilization of the NPs [63, 69], and so the 20 mL was taken as an optimum condition to study other variables. The result obtained was in close agreement with the literature [70], in which the effect of the volume of plant extract on the green synthesis of Co_3O_4 NPs was studied.

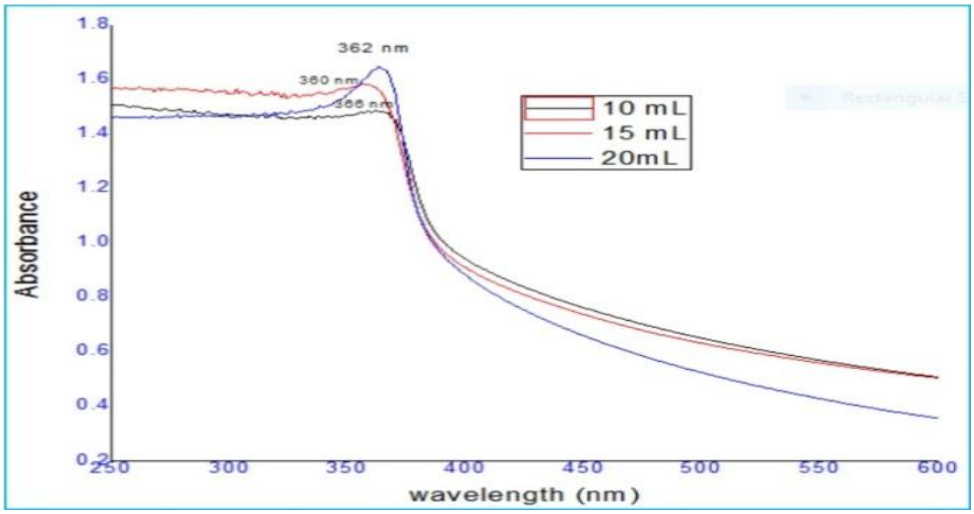

Fig 11. UV-Vis spectra of plant optimization

4. 2. 5. Concentration of Zn $(NO_3)_2.6H_2O$ Optimizations

In this study, the absorption peak was increased due to increasing concentration of Zn $(NO_3)_2.6H_2O$ solution from 0. 05 to 0. 15 M (fig. 12). This may be due to the formation of more Co/ ZnO NCs as reaction progress. Since intensity of the surface Plasmon has a direct proportionality with the density of the synthesized NPs in the solution [69]. The result obtained was in a close agreement with recent report [71] in which the effect of the concentration of cobalt nitrate on the green synthesis of Co NPs was studied. Therefore, 0. 15 M was taken as the optimized condition to biosynthesize Co/ ZnO NCs.

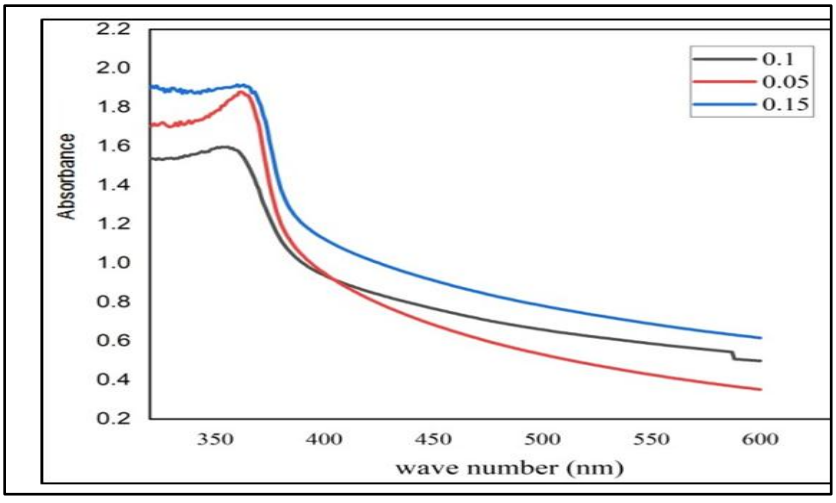

Fig 12. UV-Vis spectra of Concentration of Zn $(NO_3)_2.6H_2O$ Optimizations

4.2.6. Concentration of dopant optimization.

During this investigation, red shift was observed in the lambda range from 369 to 375 nm while the concentration of the dopant increase from 0. 01 M to 0.05 M and decreased to 362 nm when reach 0. 1 M, Which resulted in a change in the optical band gap value and therefore, 0. 05 M (5%) was taken as optimum dopant concentration to synthesize Co /ZnO NCs (fig. 13) because it gave a sharp peak at maximum wave length compared to others. A similar result was reported in the literature [57] that studied the effect of concentration of Co dopant on the surface Plasmon peak resonance of ZnO NPs.

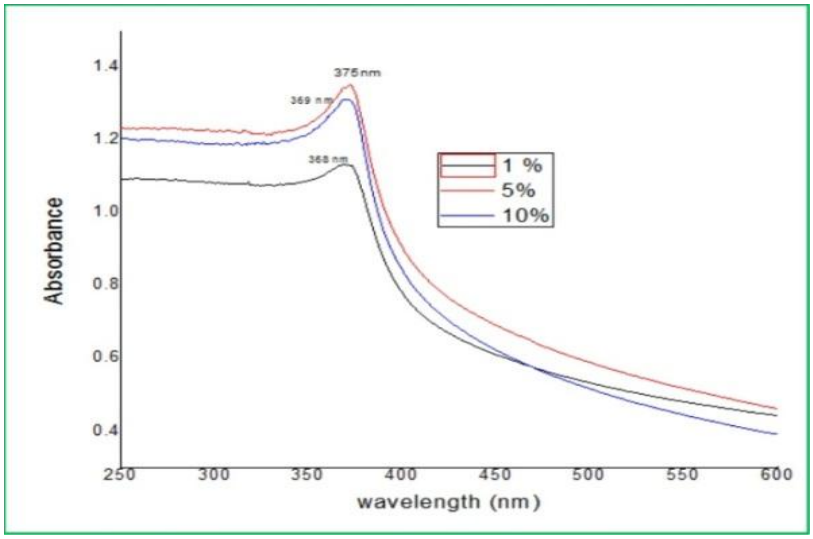

Fig 13. UV-Vis spectra of dopant concentration optimization

4. 3. Characterization of Synthesized NPs and NCs

4. 3. 1. UV-Vis spectroscopy analysis

During analysis of synthesized samples by UV-Vis spectroscopy, the absorption peak appeared at 369 and 375 nm (red shift), which confirms the formation of ZnO NPs and Co/ZnO NCs, respectively (Fig. 14).

This redshift phenomenon is mainly due to sp-d exchange interactions between the localized d electrons and the band electrons of Co^{2+} ions, which substitute Zn ions. The result obtained closely matched the recent report [23], in which Co/ZnO NCs were synthesized from Muntingia calabura leaf extract and the maximum absorption peak was obtained at 372 nm, whereas the absorption peak of ZnO NPs was obtained at 359 nm [12].

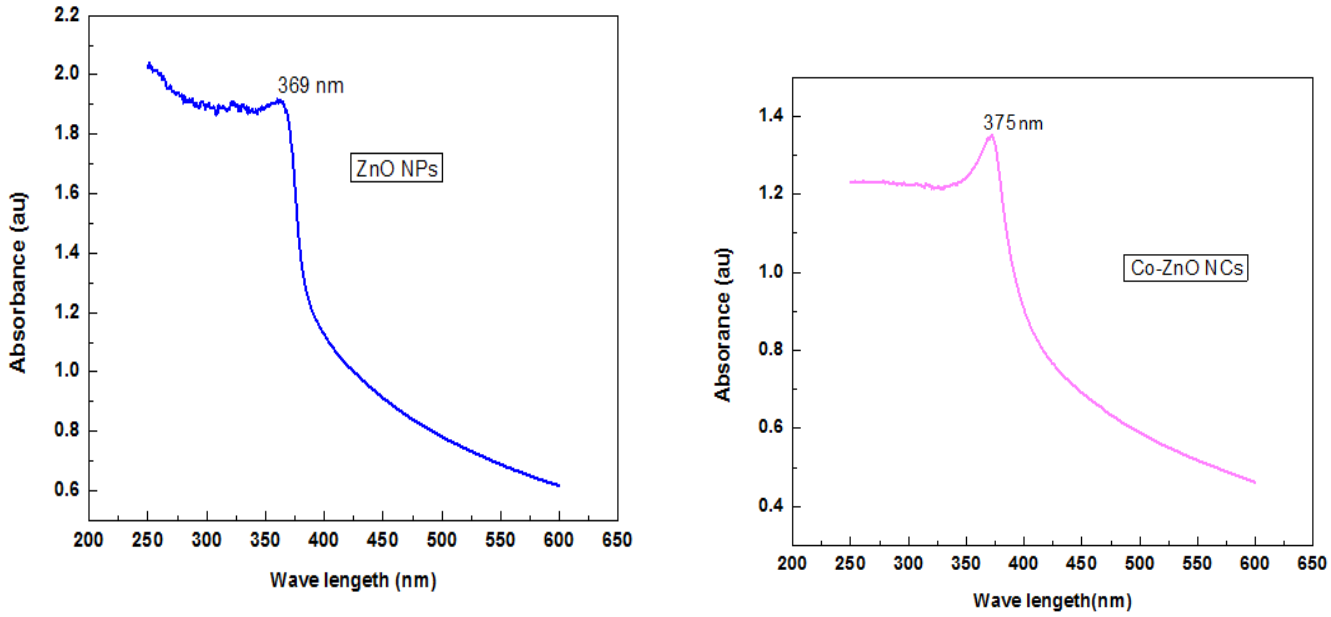

Fig 14. UV-Vis spectra of ZnO NPs (0.15M) and Co-ZnO NCs

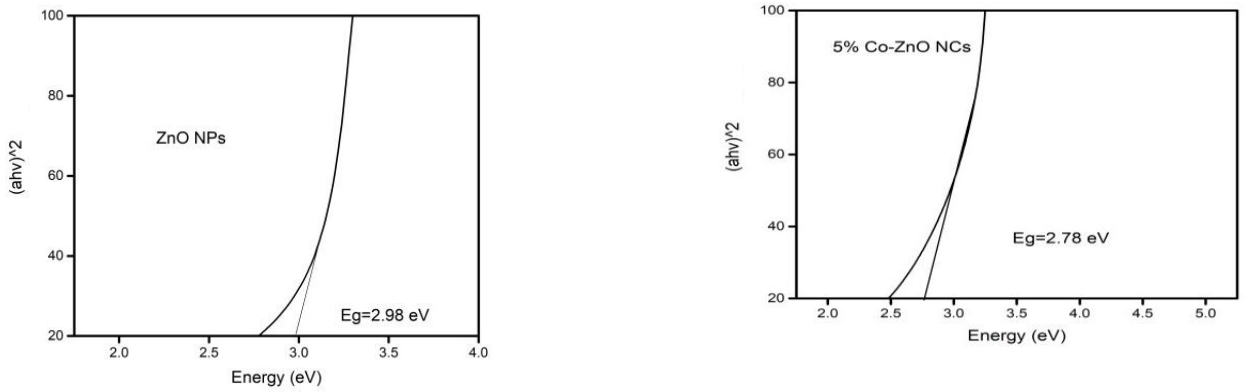

Fig 15. UV -Vis spectral band gap of (a) ZnO NPs and (b) Co/ZnO NCs

From Fig.15 a and b, the energy band gaps of green synthesized ZnO NPs and Co/ZnO NCs were 2.98 and 2.78 eV, respectively. Generally, the energy band gap of green synthesized ZnO NPs was decreased by doping cobalt to ZnO NPs, which mainly indicates improved conductance because of doping [7].

Depending on the works of the literature [23, 3, and 38], the characteristic energy band gap of ZnO NPs by doping has been reported to be between 2.97 eV and 3.1 eV, which is in close agreement with the present findings.

4.3.2. FT-IR analysis.

Fourier-transform infrared (FTIR) spectroscopy was performed for functional group analysis in the structure of the synthesized photocatalysts. Fig. 16 compares the FTIR spectra of raw ZnO and Co/ZnO samples. Some of the signals with noticeable peaks were identified and assigned to specific functional groups, as follows: The weak intensity bands at around 750–500 cm^{-1} are characteristics of metal-oxygen stretching vibrations of the Zn–O group, especially in the spectrum of raw ZnO, which almost shifts in the case of Co/ZnO. This can be associated with the incorporation of Co ions onto the ZnO surface [45].

A small and sharp peak located at 1041 cm^{-1} in the spectrum of the Co/ZnO sample is probably the C-O or C - N bond [46]. On further resolving the ZnO and Co/ZnO spectra, a small intense peak at 1009 cm^{-1} and medium intensity bands in the region of 1500–1700 cm^{-1} were observed, which are attributed to OH and H - OH bending vibrations, respectively [47]. These bands are an indication of the surface hydroxylation of photocatalysts on account of atmospheric moisture adsorption, which was further confirmed by the appearance of a broad band at 3100–3300 cm^{-1} related to OH stretching vibrational modes. The small and sharp peak observed around 1700–1800 cm^{-1} may also be due to the C=O functional group of quinones or conjugated ketone [21]. A high and sharp peak located at 3330 and 1633 cm^{-1} in the spectrum of the plant showed OH and C=C functional groups, respectively.

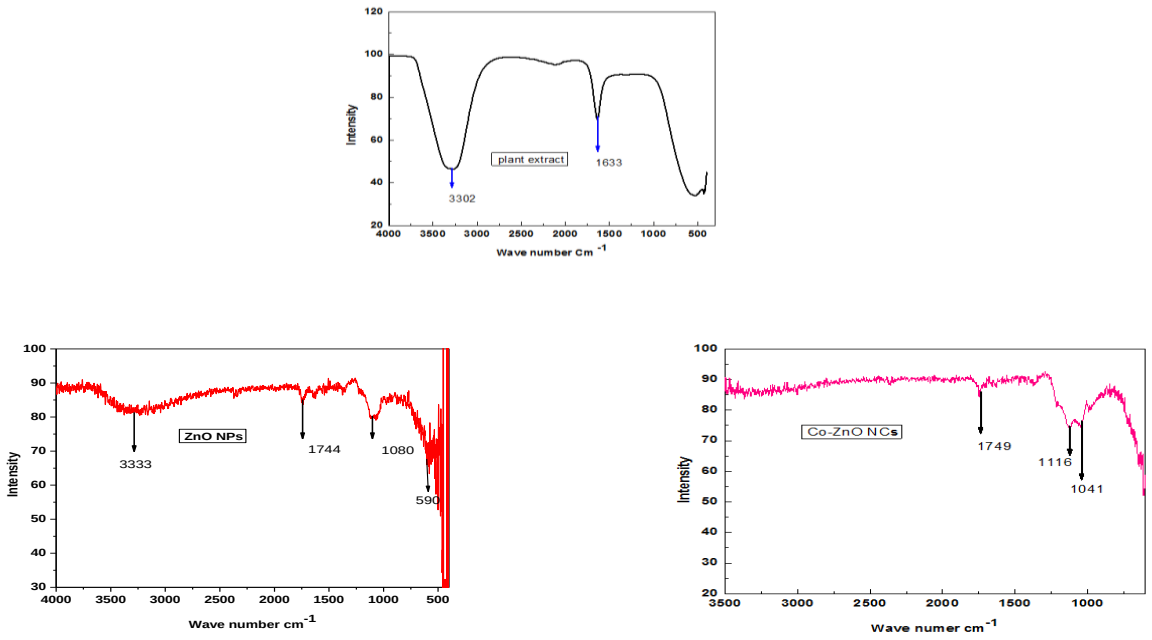

Fig 16. FT-IR results of A, Co-ZnO NCs B, ZnO NPs and C, plant

4. 3. 3 . X- Ray diffraction analysis.

XRD patterns of ZnO and Co-ZnO samples are given in Fig. 17. All the diffraction peaks match the standard diffraction data for ZnO, as expected. The XRD patterns exhibit sharp peaks at 2θ degrees 28.48, 34.40, 34.33, 36.24 , 47.56, 56.59, 62.87, and 68.07 indexed to (0 0 2), (1 0 1), (1 0 2), (1 1 0), (1 0 3), (1 1 2), (2 0 1), (0 0 4), and (2 0 2) hkl crystal planes of ZnO, respectively (JCPDS card no. 89-0510) [29]. This result was consistent with the fact that the ionic radius of Co^{2+} (0.72 Å) is less than that of Zn^{2+} (0.74 Å) [25]. In addition, NCs did not exhibit a secondary phase such as cobalt oxide. Co^{2+} partially replaced the ZnO crystal lattice without forming a secondary phase. Meanwhile, in the case of co-doped ZnO NPs, there is a shift in intensity at (101), possibly related to the effect of the substitution of Co^{2+} with the Zn^{2+} sites in the ZnO lattice and the resultant reduction of the unit cell volume. The grain size of the nanocomposite was determined using the Debye-Scherrer equation.

$$D = K\lambda / \beta \cos\theta;$$

Where K is a constant equal to 0.94 and D and λ are the particle size nanometer and wavelength of the radiation (1.54056 Å for Cu Kα radiation), respectively. β and θ are the peak width at half-maximum intensity (FWHM) and peak position, respectively. The average crystallite size of 5% Co/ZnO is found to be 27.43 nm.

The particle size of Co doped ZnO was found to be lower than that of pure ZnO (33.97 nm). It was found that the decrease in particle size was attributed to disorders created by the cobalt ions in the ZnO lattice structure. From the study, it was assumed that for a smaller amount of Co , its ions substitute well with

Zn ions. Furthermore, the peak positions were shifted to higher 2θ values, indicating possible contraction of the ZnO unit cell [10].

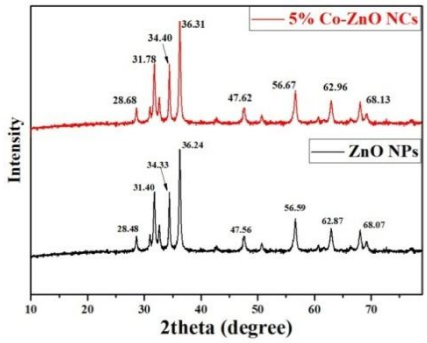

Fig 17. XRD results of ZnO NPs and 5% Co-ZnO NCs.

4.3.4. SEM analysis

ZnO NCs exhibited vertical growth as well as a homogeneous distribution morphology, in addition to a hexagonal wurthzite structure in the diameter range of 5 - 20 µm. A significant difference in shape and size for the Co/ZnO NCs was not observed, as was a relatively uniform distribution on the ZnO NPs and Co/ZnO NCs surfaces. From the presented SEM images of the Co/ZnO films, one can see from Fig. 18 that the surface of the samples obtained is also relatively porous. The SEM images demonstrate that increasing doping concentration inhibits the growth of nanostructures, which leads to the formation of structures with smaller sizes and a larger surface area.

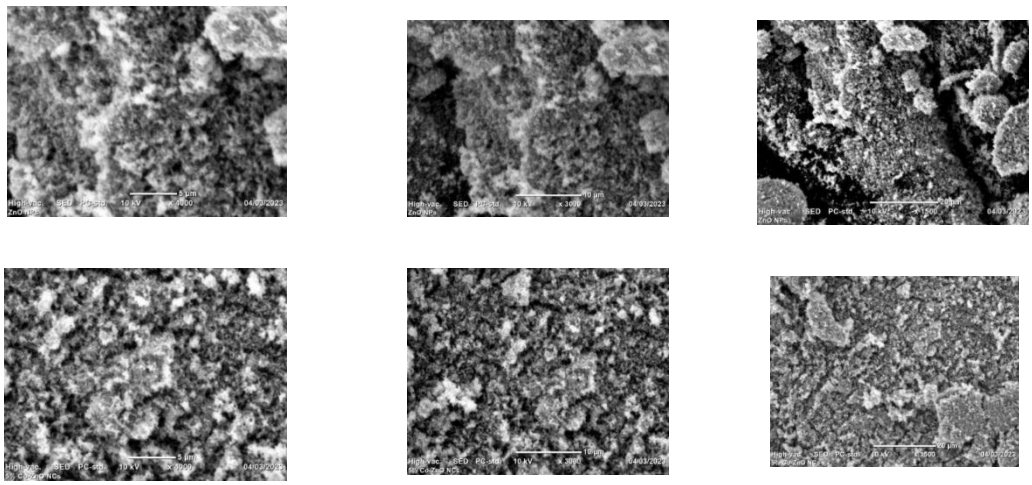

Fig 18 . SEM results of ZnO NPs and Co/ZnO NCs in the range of 5-20 micrometers .

4.3. 5 Determinations of surface charge

The pHpzc of Co / ZnO NCs was found to be 7.15 (Fig. 19). Therefore, above pH values of this, the nanocatalyst has a negative charge, and below it, it has a positive charge [29]. A similar result was reported in the literature [19]: the surface of ZnO NPs and Cu/ZnO NCs showed a negative charge and close values greater than pH 6, as they characterize the surface charge of ZnO NPs and Cu/ZnO NCs from zeta potential.

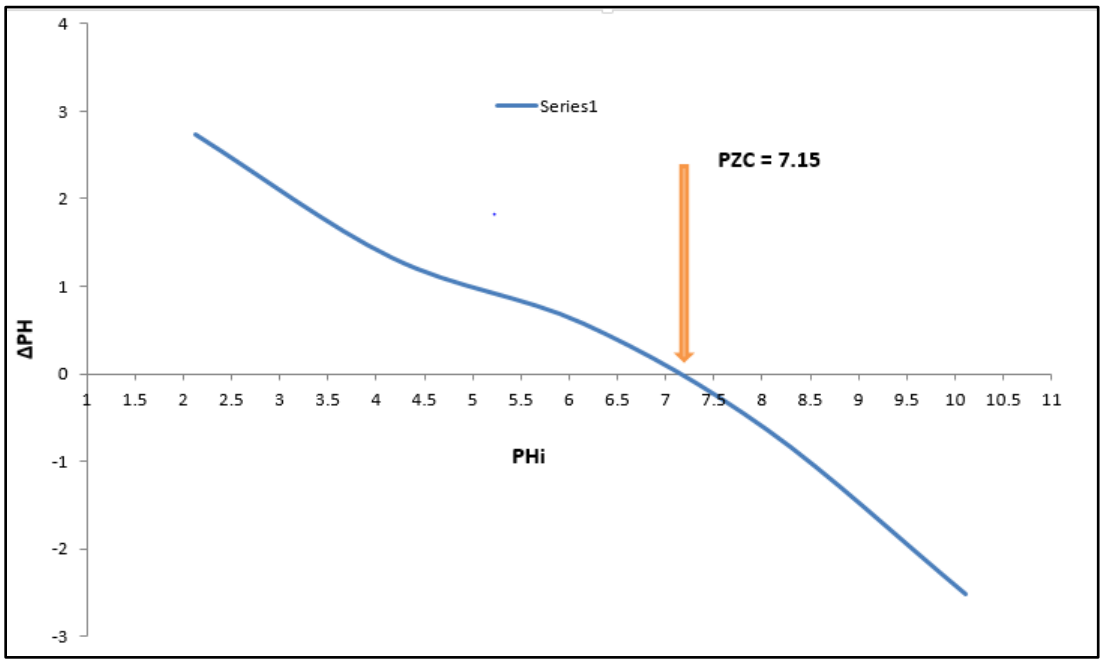

Fig 19 . Results Pzc determinations for degradation

4.4. Synthesis of ZnO NPs And Co/ ZnO NCs

During the synthesis of ZnO NPs, the color of the mixtures of plant extract and Zn $(NO_3)_2.6H_2O$ solution was reddish at the beginning. After heating for 2 hours with continued stirring at 65 oC, a white color was observed, which indicates the formation of ZnO NPs. Co/ZnO NCs were synthesized in a similar way to ZnO NPs, but the addition of Co as an impurity (dopant) and a white color were observed, which indicates the formation of Co/ZnO NCs. (Appendix 2D). The Zn and Co ions were reduced to their corresponding ZnO NPs and Co/ZnO NCs, and the synthesized NPs and NCs were templated through phytochemicals present in the plant extract [21].

4.5. Applications of synthesized NPs and NCs.

4.5.1. Photocatalytic activity.

A Optimizations of parameters for the degradation of Methyl blue dye.

a. Catalyst dosage.

With an increase in Co/ZnO nanocatalyst from 30 to 50 mg, the degradation percentage increased from 90.1 to 98% because enhancing a catalyst dosage enhances the MB dye degradation by activating active reaction sites of the nanocatalyst and reactive radicals that result in enhanced photodegradation efficiency [23]. By further increasing the catalyst dosage to 70 mg (Appendix 2E), the percentage degradation was decreased to (94.1%) due to the protection of light penetration by the catalyst surface [72, 73]. The decrease in degradation at 30 mg may be attributed to the smaller catalyst dosage, which further reduced its ability to decolorize the dye (Appendix 2E). Therefore, 50 mg (Fig. 20) of Co/ZnO NCs was taken as an optimum condition to study the effects of other parameters on the photocatalytic activity of NCs on MB dye degradation. A similar result was reported by recent literature [26, 27]: with an excess amount of a photocatalyst, degradation percentage decreased due to penetration of light protection by the nanocatalyst surface.

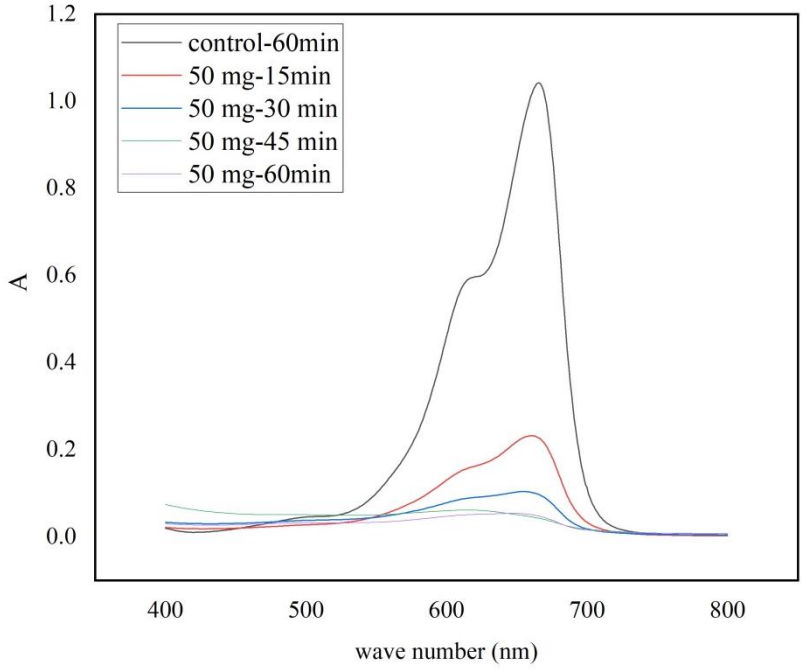

Fig 20. Dosage optimizations for Degradation result.

b. Effect of pH

At 60 min, the percentage degradation of MB dye by Co/ZnO NCs was 91.7, 98.1, and 96.5% for Co/ZnO NCs at pH values of 8, 9, and 10, respectively. From the result obtained (Fig 21), the degradation efficiency (calculated from absorbance) was increased until pH 9 (pink color), but after that it was slowly reduced because it is assumed that as pH increases, the concentration of OH^- ion also increases. Consequently, the oxidation reaction rate, which leads to OH-ion production, will increase, and dye degradation will occur at a higher rate. However, it is notable that as pH increases more and more, there are repulsive forces between the photocatalyst charged surface with negative potential and the OH-ion, which leads to a decrease in dye adsorption rate and OH radical generation that play a significant role in the degradation of dye [30]. Similar results were reported in the literature [31], in which as the pH of the solution increased more and more, the degradation efficiency decreased because of the repulsive forces between the negatively charged photocatalyst surface and OH^- ion . This study confirmed that the MB dye showed more degradation at alkaline pH, specifically at pH 9 and this was due to the adsorption of more MB dye on the surface of Co/ZnO NCs by electrostatic attraction [32]. In general, in the acidic medium, the surface of the catalyst is positively charged, and as a result, a repulsive force occurs between the photocatalyst surface and the cationic MB dye, which hinders the degradation process. This was in agreement with recently reported literature [33, 34].

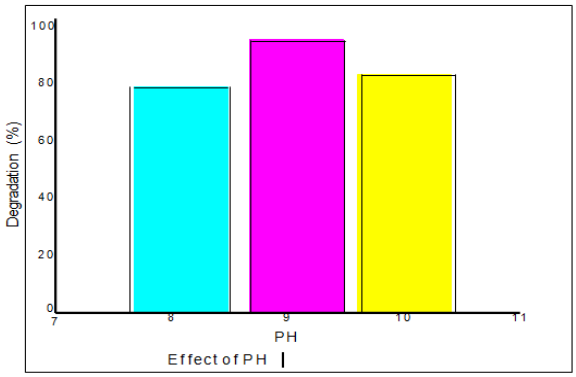

Fig 21. Effect of pH on the MB dye degradation.

c. Effect of initial dye concentration

The concentration of dye is one of the main parameters that changed the degradation efficiency in photocatalytic degradation [40]. The effect of the initial dye concentration on the decolorization of MB was studied under natural sunlight by varying the initial MB dye concentration from 10 mg/L to 30 mg/L

in the presence of 50 mg of Co/ZnO NCs at optimum pH (9), and for 60 min. The degradation percentage of MB dye decreases from 95.5 to 87.3% when the initial dye concentration reaches 10 to 30 mg/L, respectively. Similar results were reported in the literature [74, 13]: increasing the dye concentration causes dye molecules to adsorb light, and the photons never reach the Co/ZnO NCs surface. At high dye concentrations, more active sites may be covered with dye ions. This may lead to a decrease in the production of OH radicals on the surface of the catalyst, which play a significant role in dye degradation, and finally, reduced efficiency of dye removal [6, 9]. Thus, photodegradation of MB dye was found to be better at low concentrations. The concentration of dye in the decolonization of MB dye has been graphically represented in Fig. 22 below.

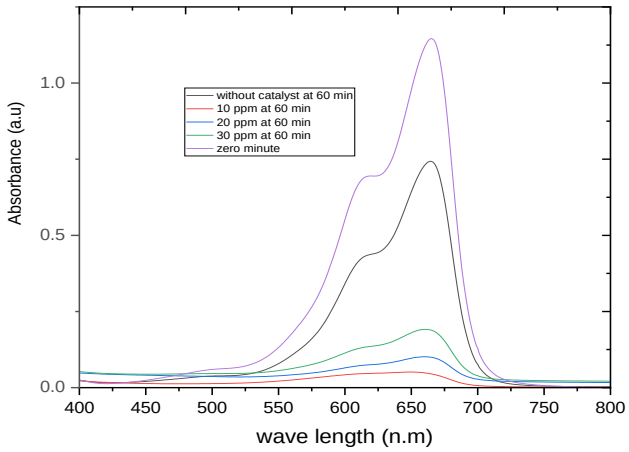

Fig 22.Concentration Optimization of MB dye (at pH =9, dose = 50 mg, 60 min).

d. Effect of irradiation time.

UV-Vis absorbance spectra were investigated to show the impact of irradiation time on the MB dye, and the highly decrement in intensity at 60 min compared to others indicates the decolorizations and demineralizations of the MB dye at this time as time goes from 15 to 60 min (Fig. 23), so 60 min was taken as the best optimum time for degradation of the MB dye according to this investigation.

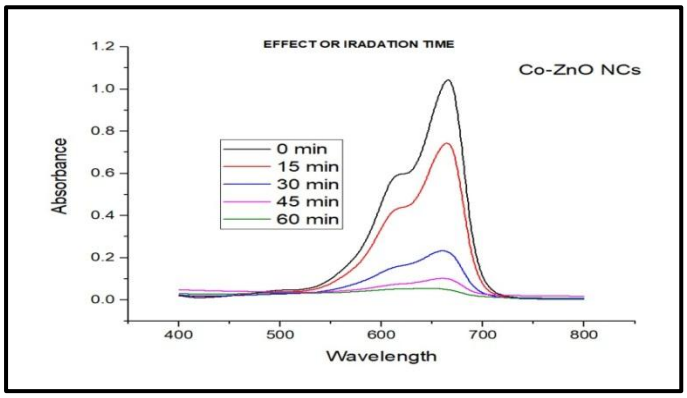

Fig 23. Effect of irradiation time on the degradation of MB dye with photocatalyst at different time interval (MB =10 mg/L , pH =9, dose = 50 mg) under natural sunlight irradiation

The percentage degradations at different time intervals from 15 to 60 min were calculated by measuring absorbance. Around 98.1% degradation efficiency was obtained by using Co/ZnO NCs at 60 min compared to the other time intervals, and additionally, the percentage degradation efficiency of ZnO NPs was 89.5% calculated at this optimum time (60 min). The better catalytic performance of Co/ZnO NCs than ZnO NPs could be due to a reduction in e^-- h^+ recombinations [27]. According to literature [35, 36], 96.1% to 84.3% of MB dyes were degraded by green synthesized Mn/ZnO NCs and ZnO NPs, which is in close agreement with this finding.

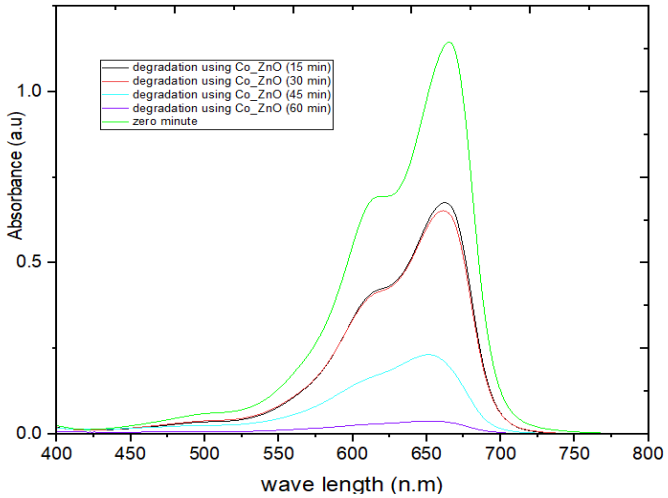

Fig 24. Degradation efficiency of Co/ZnO NCs at different time interval (10 mg/L, 50 mg, 60 min and pH 9) under natural sunlight irradiation

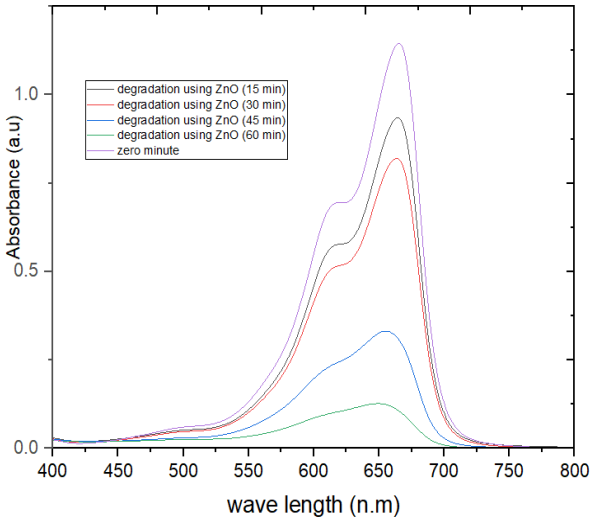

Fig 25. Degradation efficiency of ZnO NPs at different time interval (10 mg/L, 50 mg, 60 min and pH 9) under natural sunlight irradiation.

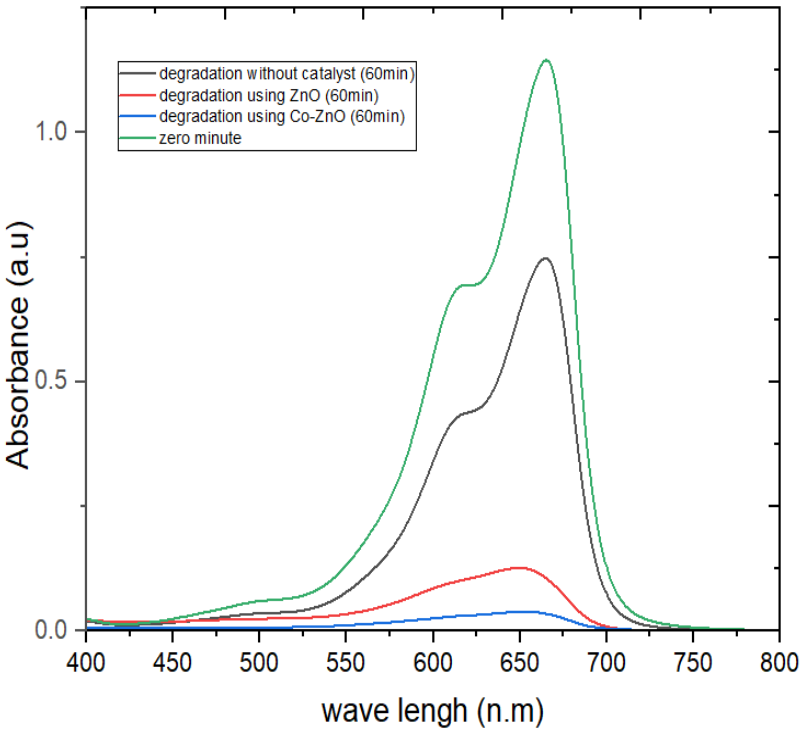

A).

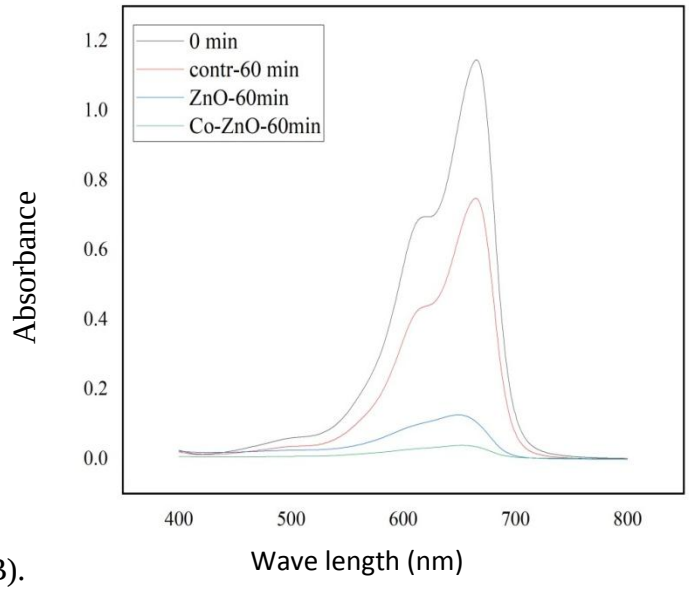

B).

Fig 26. (A and B). Degradation efficiency of (control), ZnO NPs and Co/ZnO NCs (10 mg/L, 50 mg and pH 9) under natural sunlight irradiation at optimized time, 60 min.

The degradation percentage was calculated by measuring absorbance at 60 min (Figs. 26 and 27). Around 98.5% degradation efficiency was obtained by using Co/ZnO NCs compared to the percentage degradation efficiency of pure ZnO NPs which was around 89.5% calculated at this optimum time (60 min). The better catalytic performance of Co/ZnO NCs than ZnO NPs could be due to a reduction in e^- - h^+ recombinations [27], and additionally, this is anticipated due to the presence of defects and oxygen vacancies created by Co doping inside the ZnO matrix [54]. According to literature [35, 36], 96.1% and 84.3% of MB dyes were degraded by green synthesized Mn/ZnO NCs and ZnO NPs, which is in close agreement with this finding.

On the other hand, a control experiment was conducted in which MB dye was irradiated with sunlight in the absence of a Co/ZnO NCs catalyst, as shown in Fig. 28 below. The findings showed that no major change in intensity of the absorption peak was observed, and only 31.2% of the dye degraded without catalyst. This indicates that the direct photolysis of MB dye was not very effective in the absence of a nanocatalyst. A close result was observed in the literature [37], and only 30% of MB dye was degraded without the addition of cobalt nanocatalyst.

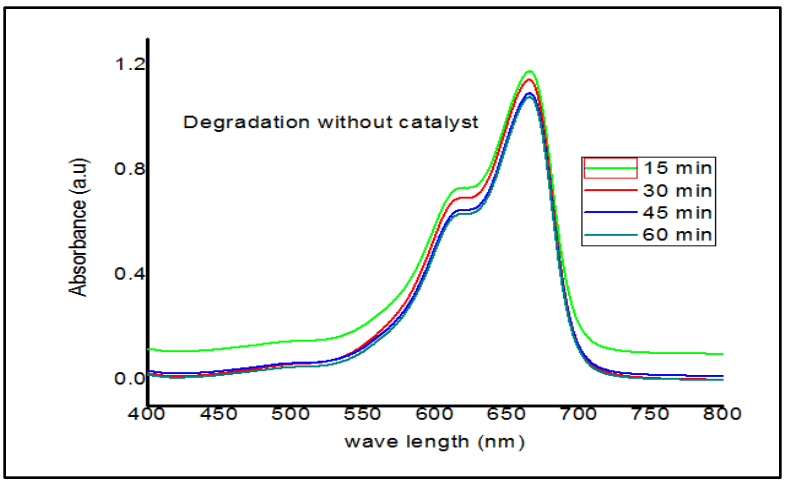

Fig 27. Degradation efficiency whithout catalyst at different time intervals (10 mg/L, 50 mg, 60 min and pH 9) under natural sunlight irradiation .

4.5.2. Reusability performance of the nanoparticles and Nanocomposites.

From Fig. 28 below, the removal of the MB dye by the ZnO NPs and Co/ZnO NCs photocatalysts after the 1st run achieved up to 95.08% and 87.99%, respectively. After the second run, the removal of the MB decreases to 90 and 85%, as well as 88 and 80% for Co/ZnO NCs and ZnO NPs, respectively, after the third round. The decrease in the removal of the MB is probably due to the loss of the recycled catalyst during sampling. From the figure, it is possible to say that ZnO NPs and Co/ZnO NCs have adequate stability and do not suffer from photo-corrosion during degradation; this is in line with reported literature [3].

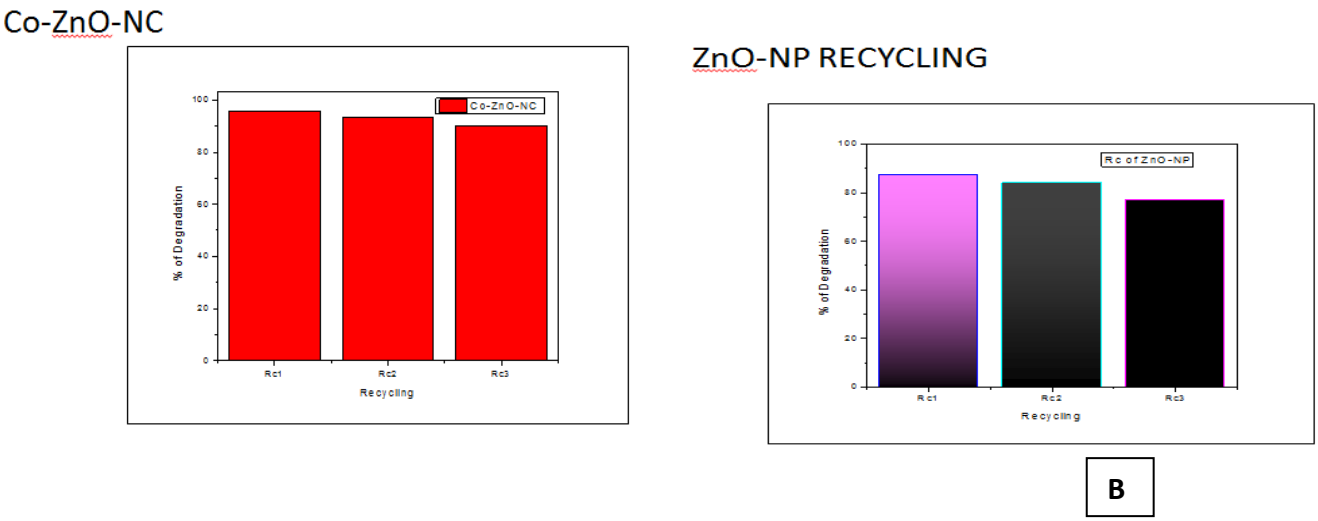

Fig 28. Recycling results of A, Co-ZnO NCs and B, ZnO NPs

4. 6. Antimicrobial activity

In this study, Co/ZnO NCs showed an adequate zone of inhibition against all microbial strains compared to ZnO NPs. The antimicrobial activity of Co/ZnO NCs is due to the high affinity of Co ions to the sulfur thrill protein of bacteria. This affinity leads to the breakage of disulfide bonds in thiols, which results in disruptions of protein tertiary structure and cell death in bacteria [41]. This finding was in agreement with [23, 43] that doping of metals (Zn, Ag, La, Ce) to ZnO NPs increases their antibacterial activity. Additionally, as concentrations of both ZnO NPs and Co/ZnO NCs increased, antibacterial activity also increased since it is concentration-dependent, which agrees with previous reports [42, 43]. The findings of this study also revealed that gram positive bacterial strains (S. aureus and B. ceurues) were more sensitive than gram negative bacterial strains (E. coli) against biosynthesized Co/ZnO NCs and ZnO NPs and towards plant extract. This variation in sensitivity and resistance to both gram negative and gram positive bacterial populations might be due to differences in their cell structure, physiology, metabolism, or degree of contact between organisms (NPs and NCs) [44]. Antibacterial activity is also size-dependent, which means as the size decreases, the surface area of the particles increases, and antibacterial activity increases [12]. The smaller the size of the particles, the higher the oxide content due to the larger surface area. The presence of oxide on the surface ensures the highest antimicrobial activity of Co/ZnO NCs and ZnO NPs, most probably due to higher concentrations of ROS, RNS, H_2O, O_2^- and OH radicals inside the microbial cell [47, 48].

The antimicrobial activity of red onion peel extract obtained from the aqueous solution against the selected microbial strains was also tested. Zones of inhibition measured against this aqueous extract were 11, 8, 10, and 9 mm for S. aureus, E. coli, B. cereus, and C. albica, respectively. The growth zone of inhibition found by plant extract is lower than that found by both ZnO NPs and Co/ZnO NCs because the synthesized NPs enhance the antimicrobial activity of the plant extract.

As both flavonoids and tannins were present as stabilizing agents on the surface of ZnO nanoparticles, they could directly interact with the fungal cell wall proteins, leading to the rupture of the cell wall. Flavonoids with different functional groups are major phytochemicals of plants and are well-known as antifungal agents,and used against a wide range of pathogenic fungi, including Candida species [75, 76]. The hydroxyl functional group position in the phenyl ring usually determines the toxicity of flavonoids against pathogenic microorganisms. Tsuchiya

et al. reported that flavonoid functional groups form a complex with extracellular proteins of the bacterial cell wall, and this complex makes the cell wall of microbial pathogens weak, resulting in a sudden stop in fungal growth [77]. Generally, the microbial effectiveness of ZnO NPs and Co/ZnO NCs has been enhanced by the development of highly reactive oxygen species like, H_2O, O_2^-, OH radicals on the surface of Co/ZnO NCs and ZnO NPs, which cause the death of microbial cells [21]. The results of the in-vitro antimicrobial activities were recorded as the average diameter of the inhibition zone in mm, which is given in Tables 3 and 4 below.

Table 3.Antimicrobial activities of biosynthesized ZnO NPs

Concentration of ZnONPs (mg/L), PE,Gentamycin, Clotrimazole	**Zone of Inhibition (mm)**			
	S.aureus	***B.Cereus***	***E.coli***	***C. albican***
100	20.1 ± 0.23	17.3 ±1.0	17.3 ± 0.7	19 ±0.6
75	16 ± 0.75	14 ±0.51	14.6 ± 0.5	16 ±0.41
50	15 ± 0.1	13.2 ±0.23	7 ± 0.5	17 ± 0.73
25	11 ± 0.4	11 ±0.3	6 ± 0.3	9 ±0.57
PE	10	7	8	8
DMSO	NI	NI	NI	NI
Gentamycin	19 ± 0.8	20.3 ± 0.5	17 ± 1.0	20 ±0.53
Clotrimazole	-	-	-	21.3 ± 0.13

Table 4.Antimicrobial activities of biosynthesized Co/ZnO NCs.

Concentration of Co/ ZnONCs (mg/L), PE,Gentamycin, Clotrimazole	**Zone of Inhibition (mm)**			
	S.aureus	***B.Cereus***	***E.coli***	***C. albican***
100	21.1 ± 0.28	20..6 ±0.15	20.3 ± 0.32	19 ±0.5
75	19 ± 0.14	15.5 ±0.7	20.6 ± 0.30	16 ±0.51
50	20 ±0.57	12.3 ±0.21	15 ± 0.10	17 ±1.1
25	19 ±0.5	10.5 ±0.5	10 ± 0.12	9 ±0.53
PE	11	10	8	9
DMSO	NI	NI	NI	NI
Gentamycin	21.4 ±0.57	20.3 ±0.53	19.5 ± 1.5	20 ±0.15
Clotrimazole	-	-	-	21.7±0.47

Key : NI no Inhibition

PE plant extract

5. CONCLUSIONS and RECOMMENDATIONS

5. 1. CONCLUSIONS

In this study, ZnO NPs and Co/ZnO NCs were successfully synthesized from $Zn(NO_3)_2.6H_2O$ and $Co(NO_3)_2.6H_2O$ using red onion peel aqeous extract as capping and reducing agents. The synthesized NPs and NCs were characterized by UV-Vis, FT-IR, SEM, and XRD. The synthesis of Co/ZnO NCs was optimized by some parameters like pH, metal ion concentration, volume of extract, temperature, and reaction time to identify the effect of those parameters on the surface of NCs. The FT-IR spectroscopy revealed the presence of possible functional groups in the synthesized ZnO NPs and Co/ZnO NCs by plant extract that were used as capping and stabilizing agents. The XRD result showed the synthesized NMs have a crystalline structure. SEM shows ZnO NPs have a spherical to wurthzite shape, and Co/ZnO NCs has a mixture of spherical shapes. The effect of parameters like pH, catalyst dosage, and dye concentration on the photocatalytic degradation of MB was studied and optimized. 50 mg of Co/ZnO NCs and pH 9 were taken as optimum conditions to study the catalytic performance of the synthesized NCs at 60 min.

Co/ZnO NCs (98.5%) showed better degradation efficiency than ZnO NPs (89.3%) at optimum conditions due to reduced e^- - h^+ recombination. Photocatalytic degradation of Co/ZnO NCs and ZnO NPs was more efficient than photolysis (degradation without catalyst). The synthesized ZnO NPs and Co/ZnO NCs have exhibited significantly greater antibacterial activity against gram-positive bacteria than gram negative bacteria due to differences in their cell structures. The synthesized ZnO NPs and Co/ZnO NCs have greater antimicrobial activity than red onion peel extract. Generally, red onion peel extract mediated green synthesis of ZnO NPs and Co/ZnO NCs has significant applications for photocatalytic degradation of MB dye and antimicrobial activity.

5. 2. RECOMMENDATIONS.

For further work, the following points were forwarded as a result of the recommendations:

1. Further characterization is required for the determination of the size and composition of the sample using instruments like TEM, Zeta Potential, XPS, and EDX.
2. Co/ZnO NCs should be applied for the degradation of other types of pollutants.

3. Further research work is needed on some other metal-doped metal oxide NCs through the remediation of red onion peel aqueous extract with an antimicrobial and photocatalytic effect.
4. Finally, the antimicrobial activity of Co/ZnO NCs against some other microbial strains should be studied.

REFERENCES

[1] Peace Saviour U. , Doga K. , Alexis N. , Saravanan S. And Saviour A. ; Biogenic Synthesis And Characterization Of Chitosan-CuO Nanocomposite And Evaluation Of Antibacterial Activity Against Gram-Positive And Gram -Negative Bacteria, **2022**, 31, 2-3.

[2] Brehan R. ; Fabrication of Copper Oxide Nanoparticles Using Endemic Plant Lippia Adoensis: Characterization, Testing and Optimization Studies, **2022,** 1, 3-5.

[3] Mohsin A. , Muhammad I. , Muhammad I. , Anwar U. , Muhammad A. and Aftab A.; Biogenic Synthesis, Characterization and Antibacterial Potential Evaluation of Copper Oxide Nanoparticles Against Escherichia coli, **2021**, 8, 3.

[6] Salah U. , Hina I. , Sirajul H. , Pervaiz A. , Mayeen Uddin K. , Hosam O. , Fatemah F., AlHarbi M. , Shaimaa A., Abdelmohsen M, andTarek K. ; Investigation of the Biological Applications of Biosynthesized Nickel Oxide Nanoparticles Mediated by Buxus wallichiana Extract,18, **2022,** 5 - 8.

[4] Anwar H., Hatim D. , Abbas Saeed H. , Ali H. and Muhammad I. ; In-Vitro Catalytic and Antibacterial Potential of Green Synthesized CuO Nanoparticles against Prevalent Multiple Drug Resistant Bovine Mastitogen Staphylococcus aureus; **2022**,25, 2.

[5] Lyimo G. ; Green Synthesised Zinc Oxide Nanoparticles and their Antifungal Effect on Candida albicans Biofilms; **2022**, 3, 2.

[7] Worku W. , Fedlu K. ,Endale T. ,Hadgu H. , and Bedasa A.; Synthesis of Copper Oxide Nanoparticles UsingPlant Leaf Extract of Catha edulis and Its Antibacterial Activity; **2020,** 6, 1.

[8]. Fozia A. ,Baharullah K., Amal A, Muhammad Q. ,Ijaz A. , Riaz U ,Mohammed B. , Anadil G. , Saira Z. and Rizwan A. ; Green Synthesis of Copper Oxide Nanoparticles Using Aervajavanica Leaf Extract and Their Characterization and Investigation of In Vitro Antimicrobial Potential and Cytotoxic Activities; **2021**, 20, 3.

[9] Mohebali H. , Mahjoub A.; Magnetic Ceria/PolyoxometalateNanocomposites and use as Photocatalysts, **2017**, 6, 1.

[10] Minas F. ; Chandravanshi, Leta S.; Chemical Precipitation Method for Chromium Removal and Its Recovery from Tannery Wastewater in Ethiopia. Chem. Int. **2017**, 3, 392−405.

[11]. Muhammad A. , Muhammad S. ,Iltaf K. , Majid M. , and Nadia A. ; Synthesis and Characterization of Co−ZnO and Evaluation of Its Photocatalytic Activity for Photodegradation of Methyl Orange; **2021**, 12, 1426.

[12]. Pradeev raj K. , Sadaiyandi K. , Kennedy A. , Suresh S. , Zaira Z. , Rafie Bin J. , Fauziah A. , Rahman F. Rafique, R. Thamiz S. and Rathina R. : Influence of Mg Doping on ZnO Nanoparticles for Enhanced Photocatalytic Evaluation and Antibacterial Analysis; **2018**,7, 3.

[13] Zahraa S. , Selma M., Jawad D, Duha S.; Influence of cobalt doping concentration on ZnO/MWCNTs hybrid prepared by sol-gel method for antibacterial activity, **2021**, 100, 117.

[14] Rania E.; Synthesis and Characterization of SomeNanostructured Materials for Visible Light-driven Photo Processes; **2020**, 25, 3.

[15] May A , Ekram Y. , Ahmad F. , Nazim H. and Maqsood A; Green Synthesis of Zinc Oxide Nanoparticles Using Salvia officinalis Leaf Extract and Their Photocatalytic and Antifungal Activities; **2021**, 10, 3.

[16] Buzuayehu A. , Enyew A. , Aschalew T. and Ananda M.; A Review on Enhancing the Antibacterial Activity of ZnO: Mechanisms and Microscopic Investigation; **2020**, 15, 3.

[17] Takuya T. , Rongliang H. , Aaron D. and Martin S.; Challenges in Determining the Location of Dopants, to Study the Influence of Metal Doping on the Photocatalytic Activities of ZnO Nanopowders:**2019**, 9, 3.

[18] Rana A. , Yadav K. , Jagadevan S.; A comprehensive review on green synthesis of nature-inspired metal nanoparticles: mechanism, application and toxicity, *J. Clean.Prod.* **2020,** 272, 122880 .

[19] Maleki P, Nemati F. , Gholoobi A. , Hashemzadeh A, Sabouri Z. , Darroudi M. , Greenfacile synthesis of silver-doped cerium oxide nanoparticles and investigation of their cytotoxicity and antibacterial activity, *Inorg. Chem. Commun.* **2021,** 131, 108762.

[20] Sevinj H. , Sezen Y. , Ekin K. ,Müjde E. , Suna S. , Büşra Y. , Tülay Ç; Evaluation of biological activities of onion from Turkey and determination of phytochemical contents, **2021**, 45, 554.

[21] Lee G. , Parks J. , Kang. H.; Quercetin, a functional compound of onion peel, remodels white adipocytes to brown-like adipocytes, *J. Nutr. Biochem*. **2017,** 42 62–71.

[22]. Khairnar S., Shrivastava V.; Facile Synthesis Of Nickel Oxide Nanoparticles For The Degradation Of Methylene Blue And Rhodamine B Dye: A Comparative Study. *J. Taibah Univ. Sci.* **2019**, 13, 1108–1118.

[23] Sara C. , Somayeh H. , Zahra G. ; Red onion skin active ingredients, extraction and biological properties for functional food applications; **2022**, 386, 2.

[24] Yaqoob A., Umar K., Ibrahim.,; Silver nanoparticles: Various methods of synthesis, size affecting factors and their potential applications—A review. Appl. Nanosci. **2020**, 10, 1369–1378. [CrossRef]

[25] Zan Y., Salmon L. , Bousseksou A.; Morphological Studies of Composite Spin Crossover@SiO2 Nanoparticles. Nanomaterials **2021**, 11, 3169. [CrossRef] [PubMed]

[26] Jarestan M., Khalatbari K., Pouraei A., Shandiz S. Beigi S., Hedayati M., Majlesi A., Akbari F., Salehzadeh A.; Preparation, characterization, and anticancer efficacy of novel cobalt oxide nanoparticles conjugated with thiosemicarbazide. *Biotech,* **2020**, 10, 1–9. [CrossRef]

[27] Puche M., Liu L., Concepción P., Sorribes I., Corma A.; Tuning the Catalytic Performance of Cobalt Nanoparticles by Tungsten Doping for Efficient and Selective Hydrogenation of Quinolines under Mild Conditions, **2021**, 11, 8197–8210. [CrossRef]

[28] Farkaš B., Terranova U., Deweras H.; The mechanism underlying the functionalization of cobalt nanoparticles by carboxylic acids: A first-principles computational study. *J. Mater. Chem. B,* **2021**, 9, 4915–4928. [CrossRef] [PubMed]

[29] De D., Upadhyay P., Das A., Ghosh A., Adhikary A., Goswami M.; Studies on cancer cell death through delivery of dopamine as anti-cancer drug by a newly functionalized cobalt ferrite nano-carrier, **2021**, 627, 127202. [CrossRef]

[30] Sirajul H. fabrication and characterization of AgO, SnO_2 and TiO_2 nanoparticles for multiple applications, **2017,** 32, 68

[32]. Mohsin A. , Muhammad I. , Muhammad I. , Anwar Ul‐Hamid, Muhammad Avais1 and Aftab Ahmad Anjum: Biogenic Synthesis, Characterization and Antibacterial Potential Evaluation of Copper Oxide Nanoparticles Against Escherichia coli; **2021**, 16, 2.

[33]. Shakeel A. , Sammia S. , Muhammad R. , Farah N. ; biogenic synthesis of CuO nanoparticles and their biomedical applications: a current review; **2017**, 5, 925.

[31] Iravani S.Varma R.; Sustainable synthesis of cobalt and cobalt oxide nanoparticles and their catalytic and biomedical applications. *Green Chem*. **2020**, 22, 2643–2661. [CrossRef]

[32] Haq S., Abbasi F., Ben Ali M., Hedfi A. Mezni A., Rehman W., Waseem M., Khan A. R., Shaheen H.; Green synthesis of cobalt oxide nanoparticles and the effect of annealing temperature on their physiochemical and biological properties. *Mater.Res. Express*, **2021**, 8, 75009. [CrossRef]

[33] Kim M., Son W., Ahn K., Kim D., Lee H.; Hydrothermal synthesis of metal nanoparticles using glycerol as a reducing agent. *J. Supercrit. Fluids* **2014**, 90, 53–59. [CrossRef]

[34] Debadrito D. , Animesh K. , Divya V. , Bapi G. , Sudha G. , Aninda M.; Assessment of photocatalytic potentiality and determination of ecotoxicity (using plant model for better environmental applicability of synthesized copper, copper oxide and copper-doped zinc oxide nanoparticles; **2017**, 12, 2.

[35]. Stanslaus G., KU L. , Revocatus L.; In situ facile green synthesis of Ag-ZnO nanocomposites using Tetradenia riperia leaf extract and its antimicrobial efficacy on water disinfection; **2022**, 24, 2.

[36] Sean D. , Tafirenyika M. and Mahabubur Ch. ; Green Synthesis Of Transition Metals Nanoparticle And Their Oxides: A Review: **2021**, 1, 2.

[37] Prashanth G. , Prabhu Ch. , Mutthuraju M. , Manoj G. , Prashanth P. , Srilatha R., Sivadhas R. , Boselin P. , Kalanakoppal V. , Holenarasipura G. , Mahmoud M. , Mohammed A. , Saurabh K. , Bharat L. And Sreeja M.; Photocatallytic Activityinduced By Metal Nano Particles Synthesized By Sustainable Approaches : A Comprehensive Review, **2022**, 10, 2.

[38] Ceren U. ; Preparation Of Multifunctional Materials For Photocatalytic Applications, **2019**, 54, 14-15.

[39] Raghavendra U. , Annamalai R. , Induja G. , Anup N. ; The Purview Of Doped Nanoparticles: Insights Into Their Biomedical Applications, **2022**, 36. 2.

[40] Abdu H. ; Review On The Synthesis Method Of Nanocomposites And Approach To Making Semiconductors Visible Light Active, **2022**, 1, 3.

[41] Keypour H. , Mahmoudabadia M.; Synthesis, Characterization and Antibacterial activity of Co(III) and Cu(II) Schiff-base complexes containing homopiperazine moiety, **2017,** 28, 23-26

[42] Naseem T, Waseem M. ; A Comprehensive Review On The Role Of Some Important Nanocomposites For Antimicrobial And Wastewater Applications, **2021,** 11, 2-5.

[43] João O. , Ailton J. , Elaine C. , Leydi J. , Otávio A. And Miryam R.; Evaluation Of Ni-Doped tricobalt tetroxide With Reduced Graphene Oxide: Structural, Photocatalysis, And Antibacterial Response, **2022**, 4, 2.

[44]. Omar M. , Muhammad A. , Suhendrayatna S. , Ismail I.; Progress of 3d metal-doped zinc oxide nanoparticle and the photocatalytic properties; **2021,** 14, 3.

[45] K. Pradeev K., Sadaiyandi A., Kennedy S. , Zaira Z. ,Mohd. Rafie Bin Johan, Fauziah Abdul Aziz, Rahman F. Rafique, R. Thamiz Selvi and R. Rathina Baal; Influence of Mg Doping on ZnO Nanoparticles for Enhanced Photocatalytic Evaluation and Antibacterial Analysis: **2018**, 31, 2-3.

[46] KhanI., Saeed K., Khan I.; Nanoparticles: Properties, Applications and Toxicities. Arab. J. Chem. 2019, 12, 908–931. [CrossRef] [46]. Correct.L. Myroniuka , D. Myroniuka, V. Karpynaa, O. Bykova ,I. Garmashevab, O. Povnitsab, L. Artiukhb K. Naumenkob, S. Zahorodniab and A. Ievtushenkoa; The Biological Activity of ZnO Nanostructures Doped by Mg and Co; **2022**, 12, 2-3.

[47] Sajid M., Płotka J.; Nanoparticles: Synthesis, Characteristics, and Applications in Analytical and Other Sciences, **2020**, 154, 104623. [CrossRef]

[48] Saleh T.; Nanomaterials: Classification, Properties, and Environmental Toxicities. *Environ. Technol. Innov*. **2020**, 20, 101067. [CrossRef]

[49] Ghosh S., Ahmad R., Zeyaullah M., Khare S.; Microbial Nano-Factories: Synthesis and Biomedical Applications, *Front. Chem*. **2021**, 9, 194. [CrossRef] [PubMed].

[50] Anuoluwapo A. , Sherine O. , And Jianjun W.; Recent trends And Advances Of Co_3o_4 Nanoparticles In Environmental Remediation Of Bacteria In Wastewater, **2022**, 12, 2.

[51] Iravani, S.; Varma, R.S. Sustainable Synthesis of Cobalt and Cobalt Oxide Nanoparticles and Their Catalytic and Biomedical Applications. Green Chem. **2020**, 22, 2643–2661. [CrossRef]

[52] Esa Y., Sapawe N.; A short review on biosynthesis of cobalt metal nanoparticles.Mater, **2020**, 31, 378–385. [CrossRef]

[53] Nadeem M. , Khan R. , Afridi K. , Nadhman A. , Ullah S. , Faisal S.; Green synthesis of cerium oxide nanoparticles (CeO_2NPs) and their antimicrobial applications: a review. *Int J Nanomed*. **2020,** 15, 5951.

[54] Kanika D. Gözde K. , Parveen Ch. , Rohit J. , Chauhan P. and Joshua O.; Biogenic Synthesis, Characterization Open Access and Antibacterial Potential Evaluation of Copper Oxide Nanoparticles Against Escherichia coli, **2021**, 6, 8-12.

[31] Aarthye, P., & Sureshkumar, M. (2021). Green synthesis of nanomaterials: An overview. Materials Today: Proceedings,**2021,** 31, 5.

[55] Bibi I., Nazar N., Iqbal M., Kamal S., Nawaz H., Nouren S., Safa Y., Jilani K., Sultan M., Ata S.; Green and eco-friendly synthesis of cobalt-oxide nanoparticle: Characterization and photo-catalytic activity. Adv. Powder Technol. **2017**, 28, 2035–2043. [CrossRef]

[56] Abdul W. , Misbahud D. , Asmat A. , Shakeeb A. , Abdul B. , Atta. , Muhammad A.; Green Fabrication Of Co And Co_3o_4 Nanoparticles And Their Biomedical Applications: A Review ; **2021**, 16, 14-17..

[57]. Arun K. Singh; A review on plant extract-based route for synthesis of cobalt nanoparticles: Photocatalytic, electrochemical sensing and antibacterial applications, **2022**, 5, 2.

[58] Zondi Nate. green synthesis of copper and silver nanoparticles andtheir antimicrobial activity, **2018**, 23, 4.

[59] Andrey A. , Parfait K. , Fedor Y. , Ivan A. , and Yaroslav M.; Current Methods for Synthesis and Potential Applications of Cobalt Nanoparticles: A Review; **2022**, 2, 3.

[60] Soruma G. Synthesis Of Nickel Oxide Nanoparticles And Copper Doped Nickel Oxide Nanocomposites Using Phytolacca Dodecandra L'herit Leaf Extract Evaluation Of Its Antioxidant And Photocatalytic Activities, **2021**, 1, 1-45.

[61] Ruth O., Hamid N., Kholijah S., Mudalip A.; phytochemical and pharmacological properties of Vernonia Amygdalina : A review. **2017**, *2*, 80–96.

[62] De O.; Synthesized and Photocatalytic Mechanism of the NiO Supported $YMnO_3$ Nanoparticles for Photocatalytic Degradation of the Methylene blue; **2019,** 3, 2-5.

[63] Nagajyothi P., Vattikuti S., Devarayapalli K. Yoo K., Sreekanth T.; Green Synthesis : Photocatalytic Degradation of Textile Dyes Using Metal and Metal Oxide Nanoparticles-Latest Trends and Advancements Green Synthesis : *Crit. Rev. Environ. Sci. Technol.*, **2019**, 5, 1–107.

[64] Xavier, S.; Lakshmi, V.; Jenila, R. M. EPRA International Journal of Research and Development (IJRD) synthesis of nio nanoparticles using thespesia populnea leaves by green, **2019**, 9, 7838.

[65] Haq S., Dildar S. Ali M., Ben M. , A. Hed A., Shahzad M.,; Antimicrobial and Antioxidant Properties of Biosynthesized of NiO Nanoparticles Using Raphanus Sativus (R . Sativus) Extract, **2021,** 11, 2-3.

[66] Khadijeh H. , Mina S. , Ahmad N. , Jamshid k.; Co-doped ZnO nanowires: Synthesis, photocatalytic performance, and cytotoxic activity against human brain glioblastoma cells, **2022**, 2, 2-3.

[67] Li J., Hong X., Wang Y., Luo, Y., Huang P., Li B., Zhang K., Zou Y, Sun L., Xu F.; Encapsulated cobalt nanoparticles as a recoverable catalyst for the hydrolysis of

sodium borohydride. Energy Storage Mater.**2020**, 27, 187–197. [CrossRef]

[68] Makiabadi M., Shamspur, T., Mostafavi A.; Performance improvement of oxygen on the carbon substrate surface for dispersion of cobalt nanoparticles and its effect on hydrogen generation rate via NaBH4 hydrolysis. *Int. J. Hydrogen Energy*, **2020**, 45, 1706–1718. [CrossRef]

[69] Xu Y., Shan W., Liang X., GAO X., Li W., Li H., Qiu X.; Cobalt Nanoparticles Encapsulated in Nitrogen-Doped Carbon Shells: Efficient and Stable Catalyst for Nitrobenzene Reduction. *Ind. Eng. Chem. Res.* **2020**, 59, 4367–4376. [CrossRef]

[70] Sharma S. ; Verma D., Khan L., Kumar S., Khan S.; Handbook of Materials Characterization, pp. 5-9.

[71] Aarthye, P., & Sureshkumar, M. (2021). Green synthesis of nanomaterials: An overview. Materials Today: Proceedings, **2021**, 4, 6.

[72] Enemali, M. O.; Udedi, S. C. Comparative Evaluation of the Protective Effect of Leaf Extracts of Vernonia Amygdalina (Bitter Leaf) and Ocimum Canum (Curry) on Acetaminophen Induced Acute Liver Toxicity.**2018**, *10*, 116–125.

[73] Saiduzzaman M. ; Synthesis And Characterization Of Cerium Doped Copper Oxide Nanoparticles By Solution Combustion Technique, **2019**, 45, 16-20.

[74]. Ceren U. ; Preparation Of Multifunctional Materials For Photocatalytic Applications, **2019**, 4, 14-15.

[75] Neeran O, and Nabel K. ; Biosynthesis of ZnO Nanoparticles in the presence of Red onion Extract, **2020**, 8, 3-8.

[76]. Shreya M., Virendra K. , Nisha Change. , Abdullah M., Anish, Abhishek K., Samreen H. , Krishna K. , Ji-Kwang Ch., and Byong-Hun J.; Onion Peel Waste Mediated-Green Synthesis of Zinc Oxide Nanoparticles and Their Phytotoxicity on Mung Bean and Wheat Plant Growth Materials **2022**, 15, 2393.

[77] Wang J., Ke Zhang D., Wang H., Zhao T., Yuan Y. Han S.; Efficient hydrolysis of alkaline sodium borohydride catalyzed by cobalt nanoparticles supported on three–dimensional graphene oxide. *Mater. Res. Bull.* **2017**, 104, 204–210 [CrossRef].

Appendix I:-pHPzc determination, MB Dye Degradation by Co-ZnO NCs, MB Dye Degradation by ZnO NPs, PzC Determination and Phytochemical tests

A

B

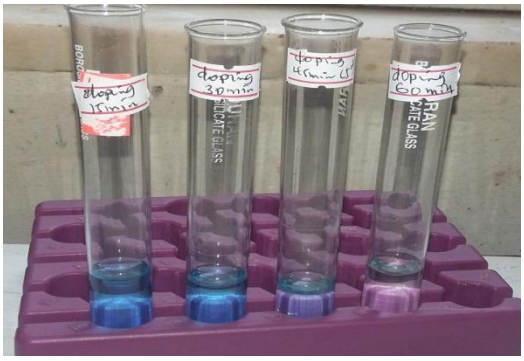

D

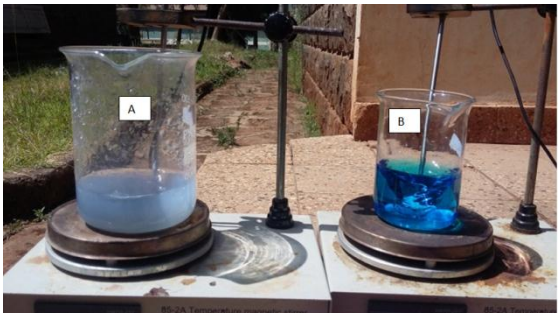

D

E

MB Dye Degradation
A, by nanocatalyst **B**, without nanocatalyst (control) under natural sunlight irradiation

Appendix II:- Degradation efficiency of Dosage optimization at constant 60 min(F&G), Degradation efficiency of at 15 to 60 min (H -K),

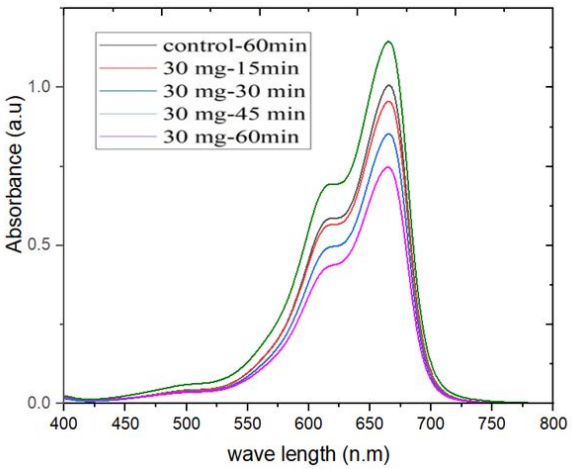

F

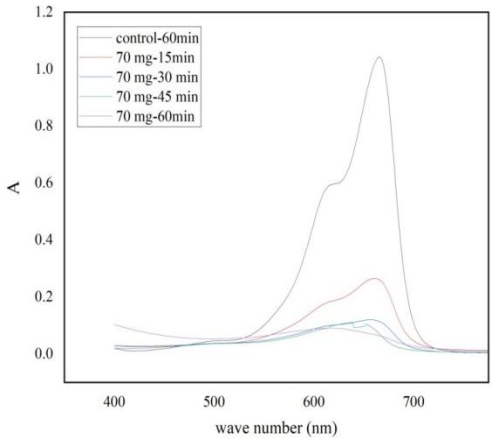

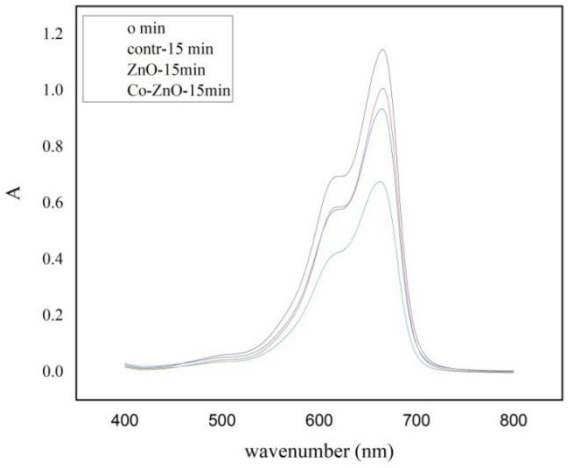

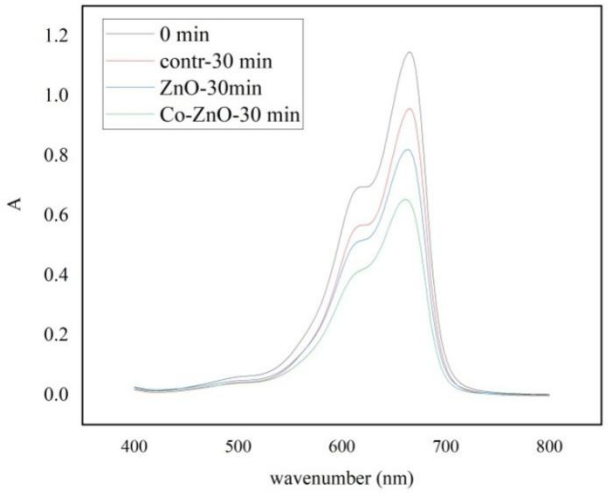

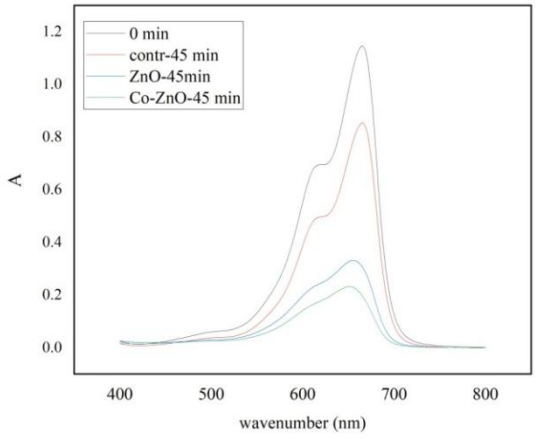

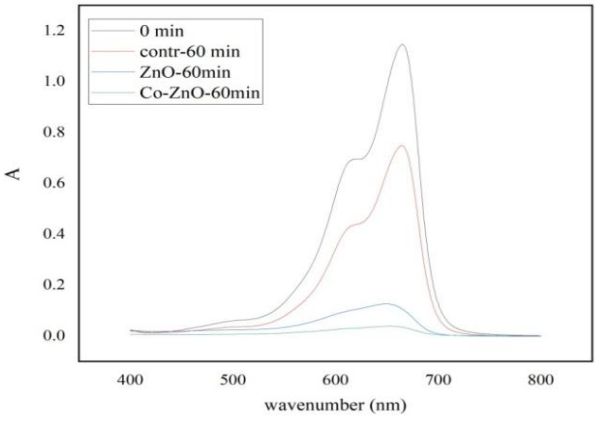

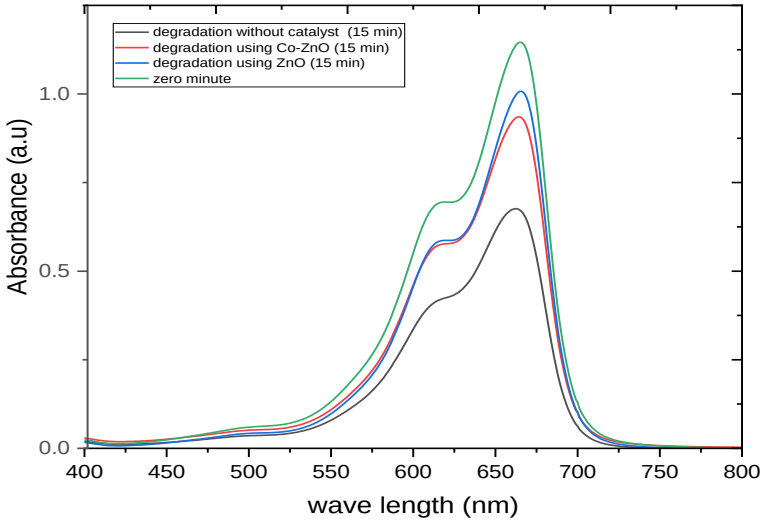
degradation without catalyst (15 min)
degradation using Co-ZnO (15 min)
degradation using ZnO (15 min)
zero minute
Absorbance (a.u)
wave length (nm)

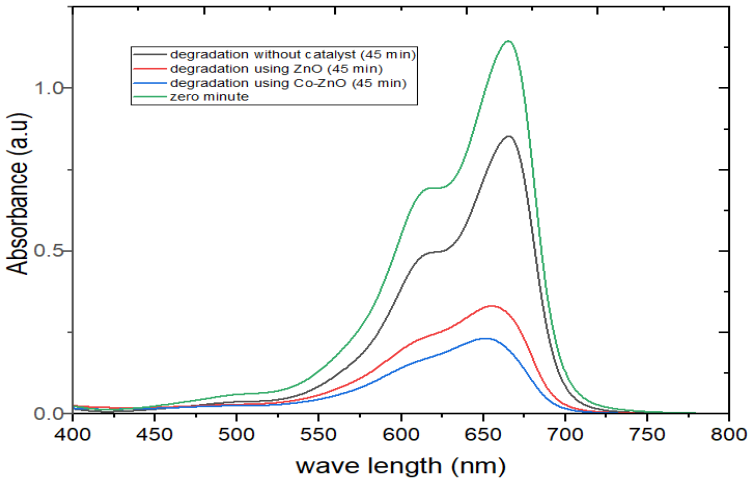
degradation without catalyst (45 min)
degradation using ZnO (45 min)
degradation using Co-ZnO (45 min)
zero minute
Absorbance (a.u)
wave length (nm)

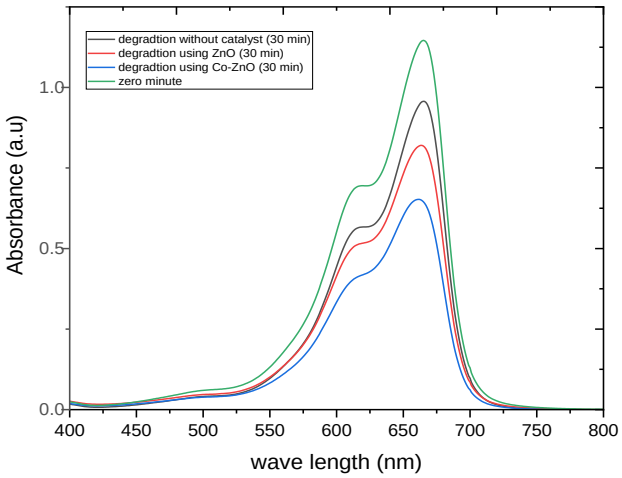
degradtion without catalyst (30 min)
degradtion using ZnO (30 min)
degradtion using Co-ZnO (30 min)
zero minute
Absorbance (a.u)
wave length (nm)

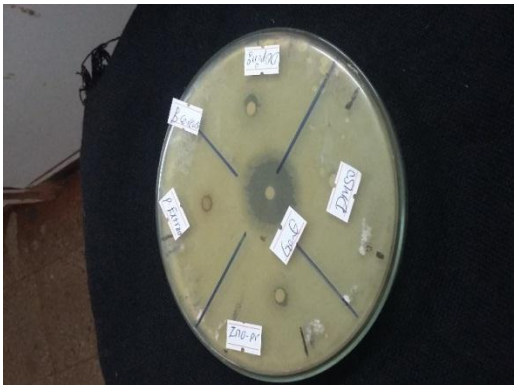

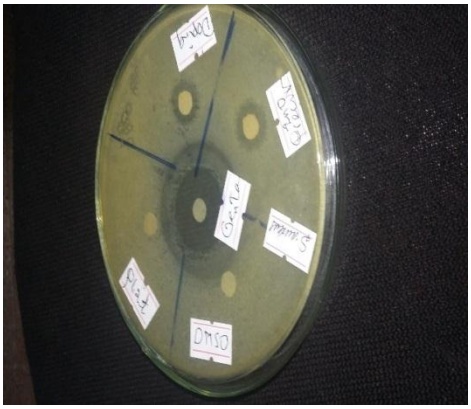

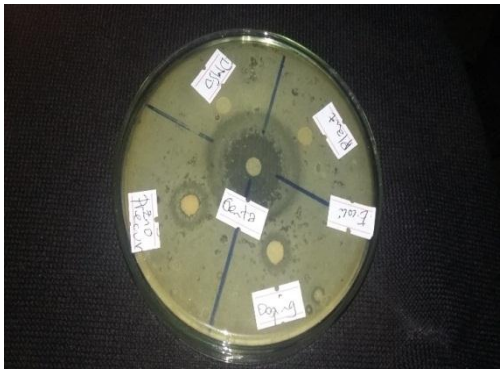

N Anti-microbial activity